UILU-ENC 86-3603

Report No. 126

FATIGUE BEHAVIOR OF GRAY CAST IRON UNDER TORSIONAL LOADS

by

Daniel Joseph Weinacht

Materials and Design Division
Department of Mechanical and Industrial Engineering

A Report of the

MATERIALS ENGINEERING - MECHANICAL BEHAVIOR

College of Engineering, University of Illinois at Urbana-Champaign

May 1986

ABSTRACT

Observations and results of constant amplitude completely reversed strain control fatigue tests are reported for a pearlitic gray cast iron. Both axial and torsional cyclic load cases have been investigated. A damage parameter based upon the product of the tensile stresses and strains ($\sigma_{max}\ \Delta\varepsilon/2$) gives good correlation of all the fatigue tests performed. The specimens employed were produced using a developmental "lost foam" casting process. Defects present in the castings had a detrimental effect on fatigue life. A continuum damage model was used to account for the influence of the defects on fatigue life. Fatigue behavior of gray cast iron castings containing large inclusions and porosities has been quantified on the basis of smooth specimen uniaxial fatigue data.

ACKNOWLEDGMENTS

I would like to acknowledge Professor Darrell F. Socie for providing a technically stimulating environment in which to pursue this work, Dr. Peter Kurath for his technical advice, and the staff of the Department of Mechanical and Industrial Engineering Publications Office for their assistance in the preparation of this document.

Deere and Company of Moline, Illinois, provided the cast iron test specimens. D. L. Brodd, L. L. Fosbinder, and S. D. Downing of the Deere Technical Center are gratefully acknowledged for their assistance throughout this investigation. Deere and the other sponsors of the Fracture Control Program also provided financial support.

My colleagues, Julie Bannantine, Jess Comer, Jay Fash, and Dan Morrow, are each recognized for the role they had in my technical development. Dave Jones is thanked for the many hours he spent polishing specimens and performing microscope work.

Finally, the largest debt I owe to my wife, Linda. Her patience, sacrifice, and support have been immeasurable.

TABLE OF CONTENTS

LIST OF TABLES

LIST OF FIGURES

Page

LIST OF SYMBOLS

a, a^*	Crack length at a given cycle number
a_f	Final crack length
a_o	Initial crack length
b	Fatigue strength exponent
c	Fatigue ductility exponent
D	Fatigue damage
D_o	Initial damage level
E	Modulus of elasticity
N	Number of applied cycles
N_f	Number of cycles to failure
P	Damage rate parameter
R_γ	Strain ratio (minimum strain/maximum strain)
R_ε	Strain ratio (minimum strain/maximum strain)
R_σ	Stress ratio (minimum stress/maximum stress)
S_y	Yield stress
$\Delta\gamma/2$	Total shear strain amplitude
ε	Strain
ε_f	True fracture ductility
ε_f'	Fatigue ductility coefficient
$\Delta\varepsilon/2$	Total strain amplitude
σ	Stress
σ_f	True fracture strength
σ_{max}	Maximum tensile stress
σ_f'	Fatigue strength coefficient
$\Delta\sigma/2$	Stress amplitude

1. INTRODUCTION

1.1 Background

Gray cast iron is one of the most widely used cast metals. The ability to be cast into intricate shapes at low cost perhaps accounts for its importance. Its name is derived from the characteristic gray color of the fracture surface of the metal which is attributed to the graphite flakes contained within the material. Several desirable characteristic properties of gray cast iron are due to the presence of the graphite flakes. These include excellent machinability, good wear resistance, resistance to galling under borderline lubrication, and excellent vibration damping.

The mechanical and physical properties of gray cast iron are strongly dependent on the nature of its microstructural components. The fact that cast irons are classified according to the shape and distribution of the free graphite particles demonstrates the importance of the carbon constituents.

Numerous researchers have investigated the deformation and uniaxial fatigue behavior of gray cast iron. Much effort has been expended in gaining an understanding of the role of the free graphite flakes. Thum and Ude [1]* utilized steel plates with various notch geometries to simulate the tensile stress-strain response of gray cast iron. Variations in the notch severity of the slots in the steel plates produced results similar to those observed in cast iron as variations are made in the graphite flake size. Coffin [2] chose to represent the graphite

* Numbers in brackets refer to entries in REFERENCES.

flakes as internal notches embedded in a ductile steel matrix. This representation allowed him to model the fracture and flow mechanism of gray cast iron.

Clough and Shank [3] reported a density decrease in cast iron during plastic deformation which they attributed to the separation of the graphite from the matrix material for properly oriented graphite flakes in a tensile stress field. They assumed this to happen in a uniform manner throughout the material resulting in an extensive internal crack network. Through several careful investigations, Gilbert [4,5,6] was able to refine the Clough and Shank assumption. Specifically, he determined that the void formation associated with the cracking and debonding of the properly oriented graphite flakes was a surface phenomenon. Gilbert claimed the interior volume changes were due to a general change in density of the graphite as opposed to crack formation.

The work of Gilbert and those who preceded him did much to explain the asymmetric stress-strain behavior of gray cast iron. They found that plastic deformation in the matrix material occurs under small tensile loadings due to the severe notch effect of the graphite flakes. Under compressive loads the graphite flakes transmit the load and their effect on material response is greatly diminished.

The efforts of Ikawa and Ohira [7] and Mitchell [8] were directed toward a determination of the effects of graphite morphology and matrix properties on the fatigue resistance of gray cast iron. Ikawa and Ohira observed fatigue cracks forming at the tips of graphite flakes oriented perpendicular to the maximum principal stress on the surface of the specimen. They also noted the cracks propagated from flake to flake and

detected multiple crack systems. Mitchell treated gray cast iron as an internally notched steel for determining fatigue resistance. In addition to stating that the fatigue resistance of gray cast iron can be enhanced by decreasing the graphite flake size, he commented on the role the matrix material has. Specifically, he claimed that the matrix hardness is an important parameter in the fatigue resistance of gray cast iron. His research revealed that decreasing matrix hardness improves fatigue resistance due to the decrease in notch sensitivity (assuming constant graphite morphology).

Fash [9] performed a detailed study of the failure/damage mechanisms of gray cast iron under uniaxial fatigue loadings. Using a surface replication procedure, he observed that crack initiation occurred very early with the majority of fatigue life being spent in the propagation and linking of multiple crack systems.

A study of the behavior of gray cast iron under compressive mean stresses was conducted by Furman [10]. No fatigue damage was observed after 10^7 cycles for fully compressive fatigue tests ($\sigma_{max} < 0$). This investigation demonstrated that tensile stresses acting on properly oriented graphite flakes are the dominant damage mechanism in gray cast iron under uniaxial loadings.

The discussion thus far indicates that Forsyth's [11] concept of a two-stage process of fatigue crack growth for wrought metals probably does not apply to the observed damage/failure process in gray cast iron. He designated crack growth in a plane of maximum shear as Stage I since it is typical of the initiation phase in wrought metals. The contention that gray cast iron is a pre-cracked material or the observa-

tion of tensile cracking very early in life seem to indicate that an initiation phase (as defined by Forsyth) is inappropriate. Crack growth on a plane of maximum shear has not been observed in gray cast iron. Rather, cracks are observed to originate from graphite flakes oriented perpendicular to the maximum principal stress and to propagate in a direction normal to the maximum principal stress. Forsyth referred to this type of crack growth as Stage II (Mode I direction in fracture mechanics terminology) since it is typical of the crack propagation phase in wrought metals. Unfortunately, many cast iron components are still designed using design codes developed for wrought materials which exhibit distinct crack initiation and propagation phases.

A parameter which accounts for the observed damage mechanism (crack growth perpendicular to the principal stress) in gray cast iron was proposed by Smith, Watson, and Topper [12]. Fash and Socie [13] successfully employed this parameter to correlate the results of uniaxial load control and strain control fatigue tests of smooth specimens under fully reversed loading conditions. Furman [10] expanded on this idea by investigating the applicability of the Smith, Watson, and Topper (SWT) parameter to test results obtained from high compressive mean stress fatigue tests. He found that the SWT parameter successfully correlated test results from high compressive mean stress fatigue tests as long as the maximum stress was tensile. The SWT parameter is undefined for fully compressive loadings ($\sigma_{max} < 0$).

In summary, the asymmetric stress-strain response of gray cast iron, as well as its characteristic fatigue behavior, is attributable to the graphite morphology. The fatigue damage process consists of crack

propagation and the linking of multiple crack systems for uniaxial loadings. The lack of any appreciable shear crack growth indicates that traditional design methodologies based on wrought metal behavior are probably inappropriate. Recent work suggests that a bulk stress-strain parameter such as that proposed by Smith, Watson, and Topper is appropriate for characterizing the damage process.

1.2 Purpose and Scope

Although numerous investigators have reported on the uniaxial deformation and fatigue behavior of gray cast iron, relatively little research has been performed with regard to the response of the material to multiaxial stress-strain states. Previous work which examines cast iron under multiaxial stress-strain conditions has been limited to studies of static fracture and flow [2,14,15,16]. It was the intent of this investigation to examine the fatigue behavior of gray cast iron under a multiaxial stress-strain state. Specifically, the fatigue properties of thin-wall tubes subjected to cyclic torsional loadings were examined.

Since fatigue damage models need to be based on the prevailing physical damage mechanisms and since the development of macroscopic crack systems has been used to quantify the damage process for uniaxial low cycle fatigue of cast iron, a qualitative study of the cracking characteristics of the gray cast iron tubes was made. The applicability of the SWT parameter to the results of torsional fatigue tests was investigated. Finally, a continuum damage model was utilized to account for the damage accumulation phenomenon in the gray cast iron tubes.

2. MATERIAL DESCRIPTION

The cast iron specimens utilized in this investigation were produced using a "lost foam" casting process currently under development at Deere and Company. The lost foam casting process involves the use of an expendable polystyrene pattern. Both a pattern and the resultant casting are portrayed in Fig. 1. Details of the casting process are proprietary and will not be presented. However, a reasonable outline of this type of investment casting can be found in Refs. [17] and [18].

The evolution of the casting process at Deere resulted in two separate batches of specimen material for this investigation. Numerous changes and improvements were made to the process between batches. A visible difference between specimens produced by the two is the surface texture as depicted in Fig. 2. One of the distinct advantages of the investment casting process is that the surface of the casting is smoother than that produced using a conventional sand casting process. This figure shows that generally a smooth surface has been achieved in the castings from the second batch. For the purposes of this investigation, the following designations were made:

Batch #1

- As-Cast Surface - CI Series
- Machined Surface - CM Series

Batch #2

- Machined Surface - NC Series

Microstructural and chemical analyses of the cast iron test bars were performed at Deere. Results of the chemical analyses are summarized in Table 1. Graphite flake structure (Figs. 3, 4, and 5) was classified using ASTM standards [19]. Classifications of the graphite flake structures and matrix microstructures are presented in Table 2. Monotonic stress-strain properties are listed in Table 3.

Large dross type casting defects were observed on the majority of the castings from both batches. Often these inclusions were present in the tube specimens even after machining. Their sizes ranged from 2 mm to 9 mm. Defects ranging in size from 2 mm to 4 mm were found frequently, while those larger than 4 mm were atypical. Examples of inclusions frequently encountered are displayed in Fig. 6 and Fig. 7. Two atypical defects are shown in Fig. 8. The average defect size was estimated to be on the order of 2 mm to 3 mm.

3. EXPERIMENTAL PROGRAM

3.1 Specimens

The tubular fatigue specimens were cast near net shape using the process discussed earlier. Tubular specimens were machined from the cast iron bars according to the dimensions given in Fig. 9. The gage sections of a number of the specimens from the first batch were left in an as-cast state (CI Series).

Figure 10 depicts the solid, smooth specimen of which a limited number were machined from the cast iron test bars of the second batch. These specimens were used both for monotonic tests and fatigue tests. In the data presentations which follow, the smooth uniaxial specimens are designated the SU Series.

3.2 Monotonic Tests

A few monotonic tests were performed using the smooth uniaxial specimen in order to establish the typical monotonic stress-strain response of the gray cast iron under investigation. This was accomplished using a 20 kip MTS servo-hydraulic test frame and a multi-user DEC 11/34 computer for control and data acquisition. A 0.5-inch gage length clip-on extensometer was used for strain measurement. Monotonic stress-strain response is depicted in Fig. 11.

3.3 Fatigue Tests

Fully reversed axial tests and fully reversed torsion tests comprised the majority of the fatigue testing which utilized the tubular specimens. Only two mean stress tests were conducted using the tubes.

An internal extensometer with 1.0-inch gage length permitted strain control testing for both axial and torsional loading conditions. Details of this extensometry are given in Ref. [20]. Though most of the tests were conducted in strain control, a few axial tests were performed in load control in the preliminary stages of the testing program.

Initially, a stiffened MTS 806 tension-torsion servo-hydraulic test frame was utilized to conduct torsion tests and axial tests. An MTS 463 processor-interface and a DEC PDP 11/23 computer performed control signal generation and data acquisition.

The final phases of testing were completed using a torsion-only machine built from an MTS 215.42 rotary actuator (20 in·kip capacity). A stand-alone dedicated controller based on the Intel 88/40 single-board digital computer handled command generation, control, and data acquisition. An adaptive feedback scheme allowed control to better than 0.1 percent resolution on full scale.

Finally, seven fully reversed axial fatigue tests were performed using the smooth specimens for comparison purposes. A clip-on extensometer allowed strain control. A 20 kip MTS servo-hydraulic test frame controlled by a stand-alone dedicated controller similar to the one described above was utilized.

Failure in the fatigue tests was defined to be 50 percent load drop or specimen separation. Normally there was little question about whether a specimen had failed. Results of the fatigue testing program are tabulated in Tables 4, 5, and 6 and graphically displayed in Figs. 12, 13, and 14.

3.4 Surface Crack Growth Observation

Since crack development in gray cast iron is regarded as the damage mechanism, it is important to monitor cracking behavior so that an appropriate damage parameter/model may be selected. An acetate tape replication procedure was used to monitor and record crack propagation at regular intervals throughout the fatigue life for a number of the tube fatigue tests. Replicas were placed between glass slides upon removal from the specimen surface. An optical microscope was used to observe the cracking behavior by transmitting light through the glass slides. The tubular specimens which were replicated were final polished using 0.3 micron alumina metallographic powder mixed in water. This eliminated machining marks on the gage section surface of the specimens. Details of the polishing and replication procedures are given by Fash [9]. The internal extensometry mentioned earlier greatly facilitated the replication process.

4. RESULTS AND DISCUSSION

4.1 Cracking Behavior

The replication procedure allowed the observation of surface crack development and propagation. The cracking behavior of the gray cast iron tubes subjected to torsional fatigue loadings was consistent with the failure mode found in the fracture and flow studies of gray cast iron performed by early researchers. Specifically, fatigue crack growth occurred on a plane perpendicular to the maximum principal stress. Observations of cracking behavior in the axial fatigue tests also parallel those made in previous investigations. In both loading situations cracks developed very early in the life (first 5 to 10 percent of fatigue life) from either properly oriented graphite flakes or the inclusions attributed to the casting process. Figure 15 displays cracks originating from graphite flakes for both axial and torsional load cases. Although this observation is consistent with the conclusions of previous investigators, it must be kept in mind that a two-dimensional view of a three-dimensional process is portrayed in these photographs. Crack growth into the surface is also a viable process.

The defects present in this material played a major role in its fatigue behavior. Typical defects included burnt-in sand on the as-cast surfaces, internal patches of a white ashen substance, and internal porosities. Frequently, cracks were observed to initiate at the surface defects. This has been documented for both axial and torsional load cases in Figs. 16 and 17. Observation of fracture surfaces following fatigue tests revealed inclusions that sometimes extended across the wall thickness of the specimen. Average defect size was estimated to be in the 2 mm to 3 mm range.

The majority of fatigue life (90 to 95 percent of fatigue life) was spent in propagation and linking of multiple crack systems. In all cases, cracks were observed to grow perpendicular to the maximum principal stress. Crack growth for an axial test and two torsion tests is tracked in Figs. 18, 19, and 20. Fash [9] found the development and linking of multiple crack systems to correlate closely with the tensile load drops observed throughout uniaxial constant amplitude strain control fatigue tests using smooth specimens. Similar behavior was observed in the tube tests for both axial and torsional loadings. Hysteresis response for an axial test (Fig. 21) indicates that very limited tensile-load-carrying ability exists immediately prior to failure. Analogous behavior is observed for the torsion tests as displayed in Figs. 22, 23, and 24. This phenomenon is interpreted in a qualitative sense to represent the accumulation of fatigue damage (cracks) in this class of material.

4.2 SWT Parameter

The parameter proposed by Smith, Watson, and Topper "is based on the hypothesis that there is a simple stress-strain function governing the fatigue of metals" [12]. The product of the maximum tensile stress (σ_{max}) and the strain amplitude ($\Delta\varepsilon/2$) is the parameter they propose.

Previous investigations have identified the SWT parameter as appropriate for the correlation of gray cast iron uniaxial fatigue data. It has been successfully applied to both completely reversed cyclic test results and mean stress test results for smooth fatigue specimens. The

most general formulation of the SWT parameter is given below

$$\sigma_{max} \frac{\Delta\varepsilon}{2} = \frac{\sigma_f'^2}{E} (2N_f)^{2b} + \sigma_f' \varepsilon_f' (2N_f)^{b+c} \qquad (1)$$

where b is the fatigue strength exponent and c is the fatigue ductility exponent. Its success in correlating data in previous investigations has been attributed to the bulk stress-strain terms more accurately representing the driving force behind crack propagation.

The cracking behavior observed in the gray cast iron tubes indicates that cast iron is sensitive to tensile stresses and, therefore, the SWT parameter should be appropriate.

For the torsional loading case, the maximum principal stresses and strains are oriented normal to a plane that is 45 degrees from the specimen axis. The maximum principal stress and strain act in a direction parallel to the specimen axis for the axial loading case. The SWT parameter was calculated for each of the fatigue tests performed (both torsion and axial) by solving for the principal stresses and strains. Presentation of all fatigue data from this investigation using the SWT parameter is portrayed in Fig. 25. The large scatter of the data is attributed to the inclusions present in the tube specimens and will be accounted for shortly. Note that the solid data points (SU Series) which represent the smooth uniaxial specimens are on the high side of the scatter. Since these specimens were machined from the center of the castings, they were free from the casting defects typical of the tube specimens. In fact, Fig. 26 demonstrates that the SU Series data points

are correlated with the following relationship

$$\sigma_{max}\ \Delta\varepsilon/2 = 1.82\ (N_f)^{-0.25} \qquad (2)$$

determined by Fash and Socie [13] for smooth specimens of a similar gray cast iron.

4.3 Damage Model

A continuum damage model examined by Downing [21] was used to account for the role of the inclusions in the fatigue life of the tube specimens. This continuum damage model replaces the linear damage model (Miner's rule) that is commonly used for wrought metals. Since the damage process in gray cast iron is typically characterized by the crack growth process, treating the inclusions present as initial crack-like defects seemed a logical approach. The damage parameter chosen was based on crack length and is defined as

$$D = {a^*}/{a_f} \qquad (3)$$

where a* is the length of the failure crack at a given point in life and a_f is the final failure crack length.

Defining damage with the above parameter allowed the initial damage attributed to the defects to be quantified. The basic concept is illustrated in Fig. 27 where the initial damage level associated with the average defect size (2 mm) is shown to consume varying portions of fatigue life for different strain amplitudes. For example, at the

higher strain, the life would be reduced by 45 percent and an 80 percent reduction in life would be expected for the same size defect at the lower strain level.

The differential equation which expresses the damage process was developed by Lemaitre and Plumtree [22] and is given below

$$\frac{dD}{dN} = \frac{(1-D)^{-P}}{(P+1)N_f}. \tag{4}$$

The damage rate accumulation parameter, P, was found to correlate with the SWT parameter, $\sigma_{max}\ \Delta\epsilon/2$, through the following relationship

$$P = 2.55\ (\sigma_{max}\ \Delta\epsilon/2)^{-0.8} \tag{5}$$

by Socie, et al. [23].

Integration of Eq. (4) yields

$$(1-D_o)^{P+1} - (1-D)^{P+1} = N/N_f \tag{6}$$

where D_o is some initial damage level associated with the inclusion size. Calculation of fatigue life assuming an initial defect size can be accomplished through the following equation (a simplified version of Eq. (6))

$$(1 - a_o/a_f)^{P+1} = N/N_f \tag{7}$$

and Eqs. (2) and (5). Note that Eq. (7) allows a quantitative analysis of the concept illustrated in Fig. 27. The quantity on the left-hand side of this equation is a reduction factor which results in the calculation of a reduced fatigue life (N) due to the non-zero initial damage level.

Using the estimated average defect size of 2 mm as a_0 and a final crack length (a_f) of 20 mm (very typical for gray cast iron) the reduced fatigue lives were calculated. Figure 28 displays the fit from the Fash-Socie relationship as well as the calculated lives assuming a 2 mm defect is initially present. The 2 mm initial defect line fits the tubular specimen fatigue data quite well. This indicates that this continuum damage model can be employed to assess the fatigue behavior of a casting given baseline smooth specimen fatigue data and an estimate of the size of defects typically found in the castings.

5. CONCLUSIONS

The fatigue behavior of gray cast iron tubes under both torsional and axial loadings has been investigated. The conclusions of this research follow:

1. Cracks are observed to initiate from properly oriented graphite flakes or inclusions very early in life. The propagation and linking of multiple crack systems constitute the majority of low cycle fatigue life in gray cast iron for both the axial and the torsional load cases. The crack growth has been observed to be on planes perpendicular to the maximum tensile stress.
2. Degradation of the tensile load-carrying ability of the material is attributed to the damage process (crack propagation) and not to cyclic softening.
3. The bulk stress-strain parameter proposed by Smith, Watson, and Topper does a reasonable job of correlating the low cycle fatigue behavior of gray cast iron tubes subjected to torsion and axial loadings.
4. Defects present in the gray cast iron specimens had a pronounced detrimental effect on fatigue lives. They ranged in size from 2 mm to 9 mm. Average defect size was estimated to be 2 mm to 3 mm.
5. A continuum damage model has been used to account for the effect of defects on fatigue life. Fatigue behavior of gray cast iron castings containing large inclusions and porosities has been quantified on the basis of smooth specimen uniaxial fatigue data.

Table 1 Material Chemistry

Series	C	Mn	P	S	Si	Ni	Cr	Mo	Cu
CM	3.65	0.39	0.016	0.067	2.30	0.11	0.04	0.02	0.12
CI	3.76	0.32	0.037	0.058	2.18	0.11	0.15	0.02	0.10
NC	3.48	0.56	0.037	0.069	1.87	0.09	0.20	0.02	0.14

Hardness

CM Series	137 BHN
CI Series	174 BHN
NC Series	212 BHN

Table 2 Material Microstructure

Series	Graphite Type	Graphite Size	Matrix
CM	A	1-2	Lamillar pearlite with 5-10% free ferrite
CI	A	2-3	Lamillar pearlite with traces of ferrite, steadite and carbide
NC	A	3-4	Lamillar pearlite with traces of ferrite and steadite
	D,E (Small Amounts)	6	

Table 3 Typical Stress-Strain Properties

Modulus of Elasticity, E (Tension/Compression)	78 GPa/103 GPa
Yield Strength, 0.2% S_y	215 MPa
Ultimate Strength (True Fracture Strength, σ_f)	260 MPa
True Fracture Ductility, ε_f	0.0076

Table 4 Axial Fatigue Data for Smooth Specimens

Specimen No.	$\Delta\varepsilon/2$	R_ε	$\Delta\sigma/2$ (MPa)	R_σ	σ_{max} (MPa)	N_f (cycles)
SU02	0.0035	-1	-	-	199	101
SU01	0.002	-1	-	-	126	2610
SU03	0.0015	-1	-	-	126	4490
SU04	0.001	-1	-	-	108	11040
SU09	0.0008	-1	-	-	81	106930
SU10	0.00075	-1	-	-	78	303070
SU08	0.0007	-1	-	-	72	693450

Table 5 Axial Fatigue Data for Tube Specimens

Specimen No.	$\Delta\varepsilon/2$	R_ε	$\Delta\sigma/2$ (MPa)	R_σ	σ_{max} (MPa)	N_f (cycles)
CI07	0.0015	-1	-	-	103	1510
CI10	0.0015	-1	-	-	88	1690
CI08	0.001	-1	-	-	64	21630
CI09	0.001	-1	-	-	80	19830
CI06	-	-	100	-1	100	6660
CI11	-	-	100	-1	100	24950
CI02	-	-	75	-1	75	51590
CI03	-	-	75	-1	75	37280
CI04	-	-	62	-1	62	52170
CI05	-	-	62	-1	62	98700
CI01	-	-	53	-1	53	$>2.60 \times 10^6$
CM18	0.0015	-1	-	-	68	4650
CM17	0.0009	-1	-	-	80	19870
CM20	0.0009	-1	-	-	57	47920
CM21	-	-	85	-1	85	29260
CM08	-	-	75	-1	75	47950
CM12	-	-	62	-1	62	65690
CM15	-	-	58	-1	58	$>1.00 \times 10^7$

Table 5 (Cont'd) Axial Fatigue Data for Tube Specimens

Specimen No.	$\Delta\varepsilon/2$	R_ε	$\Delta\sigma/2$ (MPa)	R_σ	σ_{max} (MPa)	N_f (cycles)
NC04	0.0035	-1	-	-	184	106
NC15	0.002	-1	-	-	182	484
NC18	0.002	-1	-	-	150	1340
NC19	0.0015	-1	-	-	132	6100
NC17	0.001	-1	-	-	99	15170
NC13	0.0007	-1	-	-	124	24800
NC14	0.0007	-1	-	-	109	22410
NC16	0.0007	-1	-	-	76	$>1.00 \times 10^6$

25 mm

Batch #1

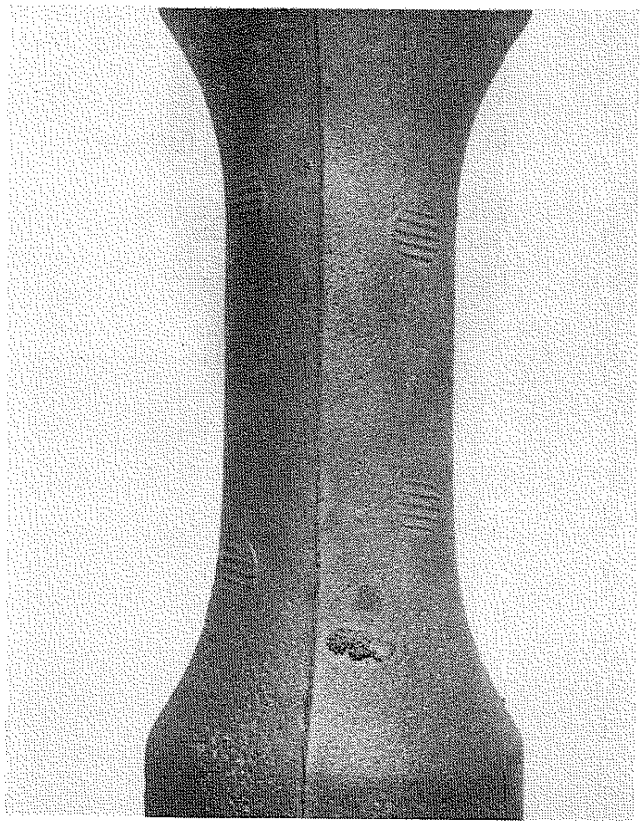

25 mm

Batch #2

Figure 2 Casting Surface Textures

0.25 mm
Picral Etch

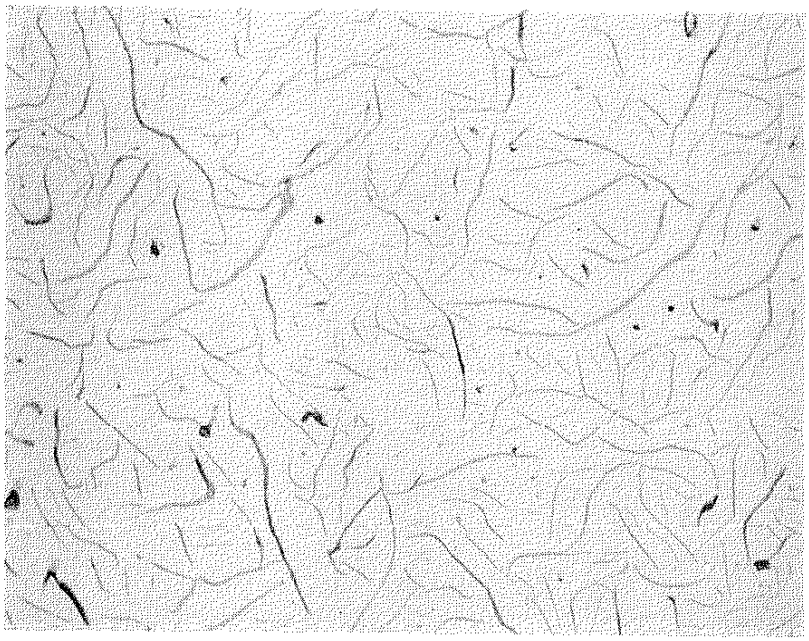

0.5 mm
Unetched

Figure 3 Microstructure - CI Series

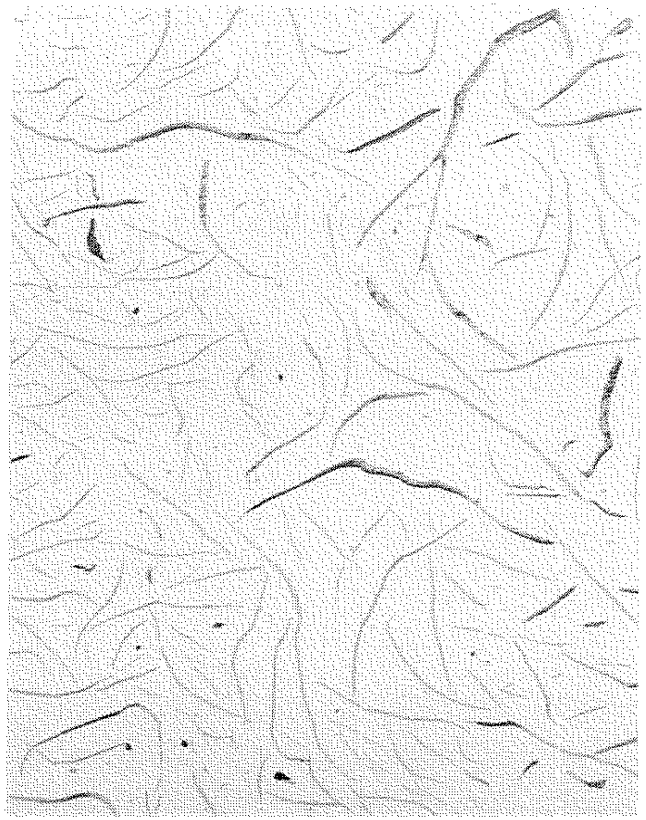

0.5 mm

Unetched

0.25 mm

Picral Etch

Figure 4 Microstructure - CM Series

0.10 mm
Picral Etch

0.5 mm
Unetched

Figure 5 Microstructure - NC Series

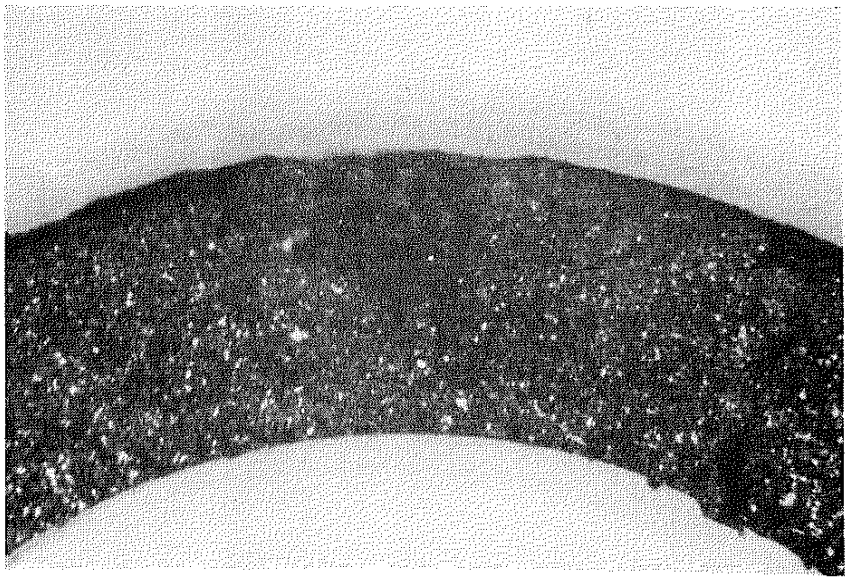

Fracture Surface - CI08
Defect #1

1.0 mm

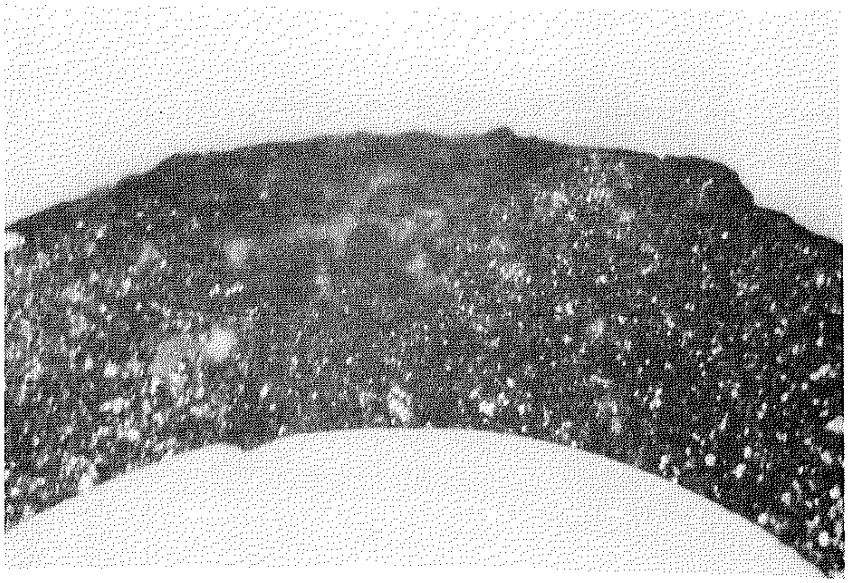

Fracture Surface - CI08
Defect #2

1.0 mm

Figure 6 Typical Defects - CI08

Fracture Surface - CM08
Defect #1

1.0 mm

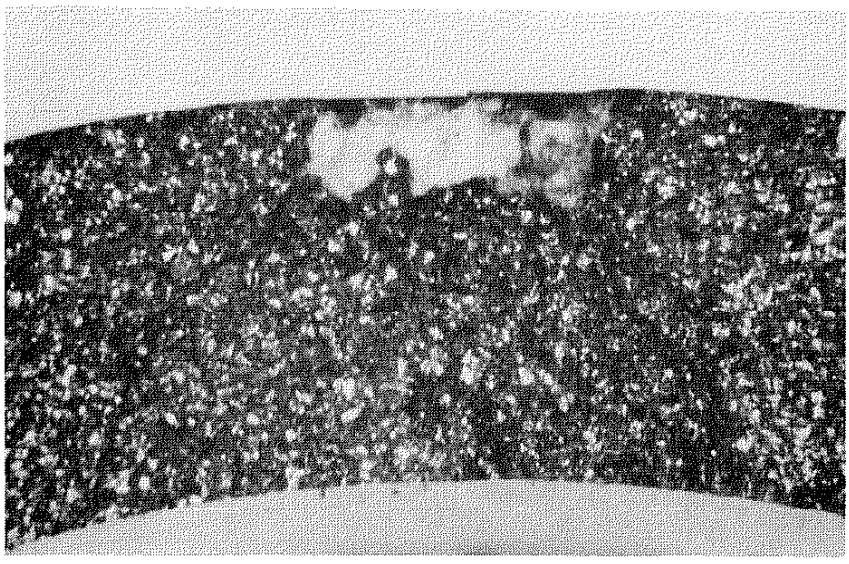

Fracture Surface - CM08
Defect #2

1.0 mm

Figure 7 Typical Defects - CM08

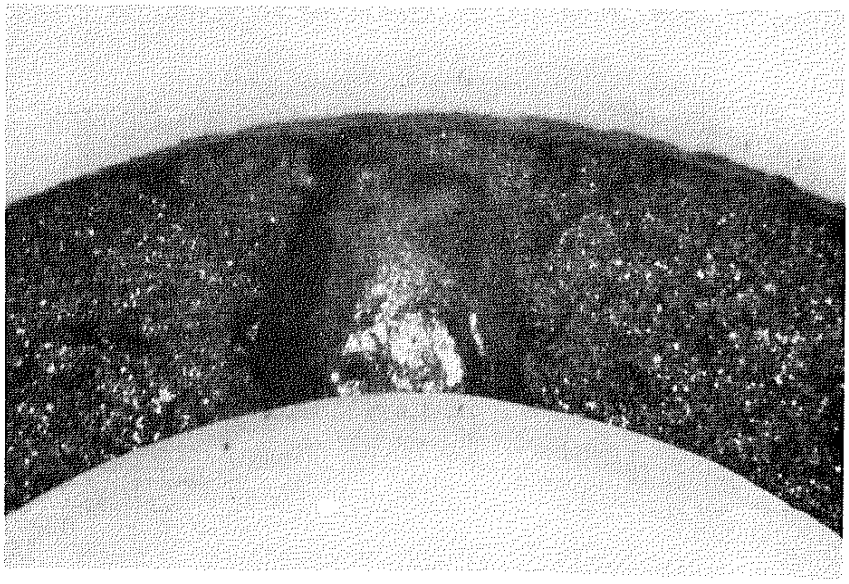

Fracture Surface - CIO2

1.0 mm

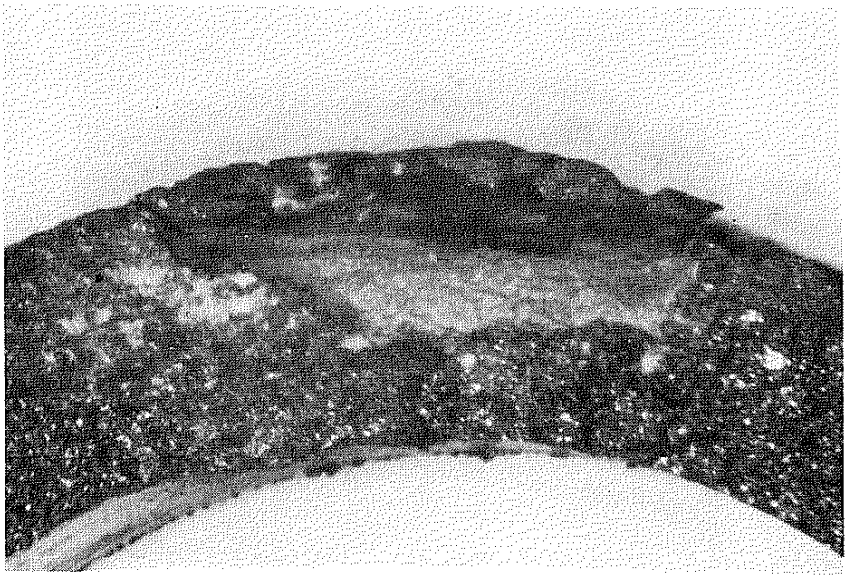

Fracture Surface - CIO3

1.0 mm

Figure 8 Atypical Defects

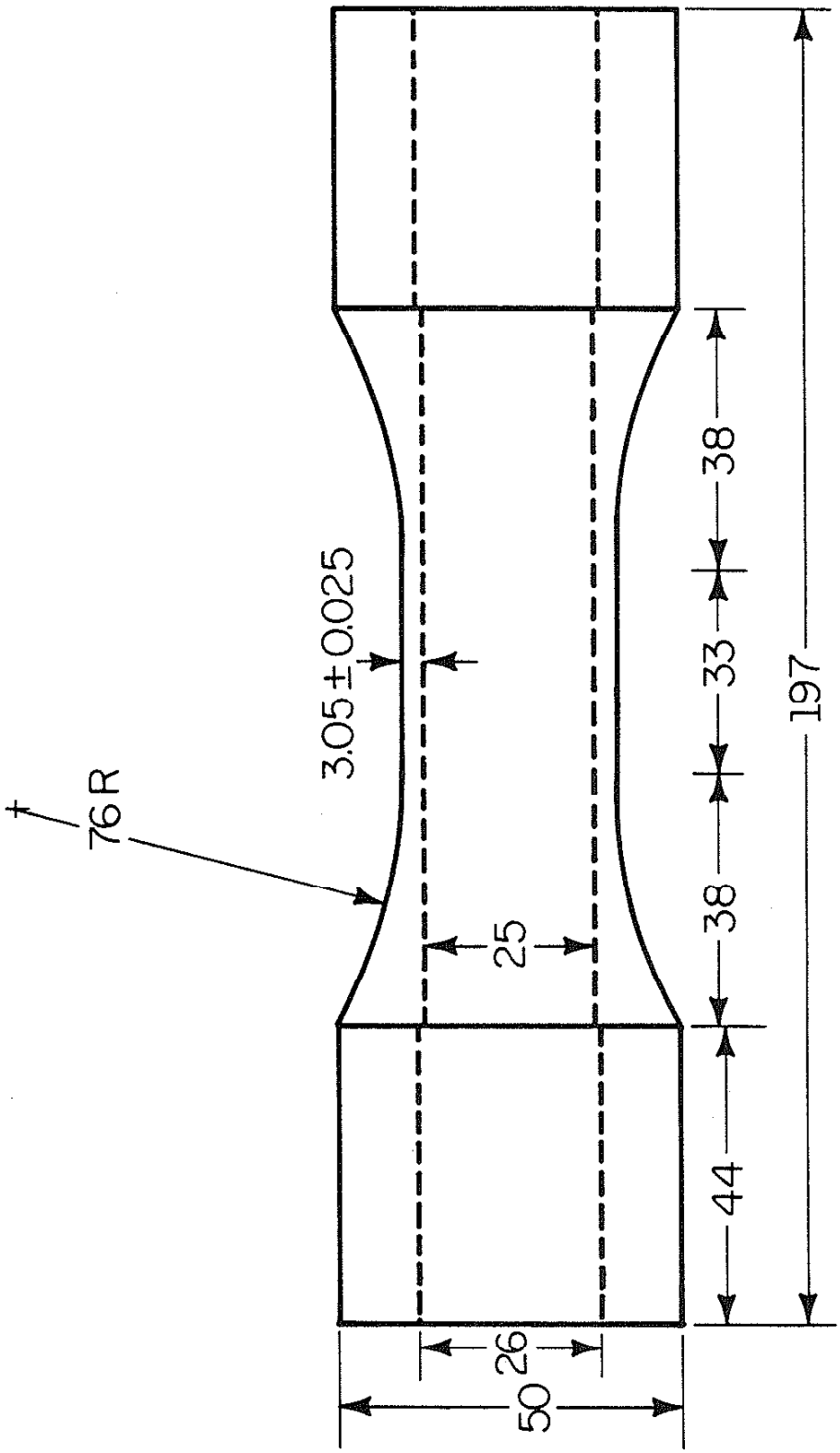

Figure 9 Tubular Specimen

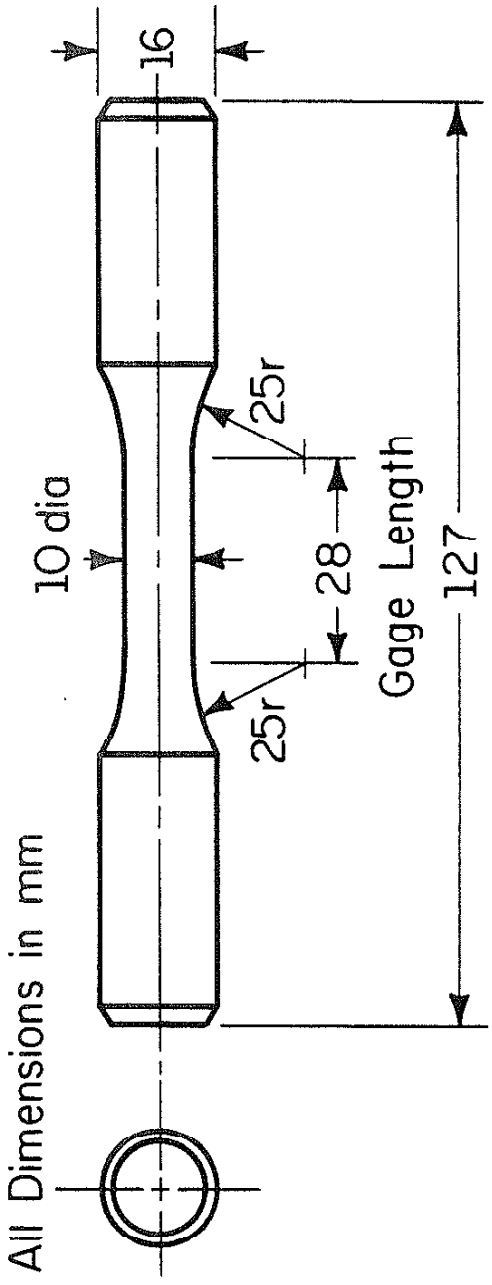

Figure 10 Uniaxial Specimen

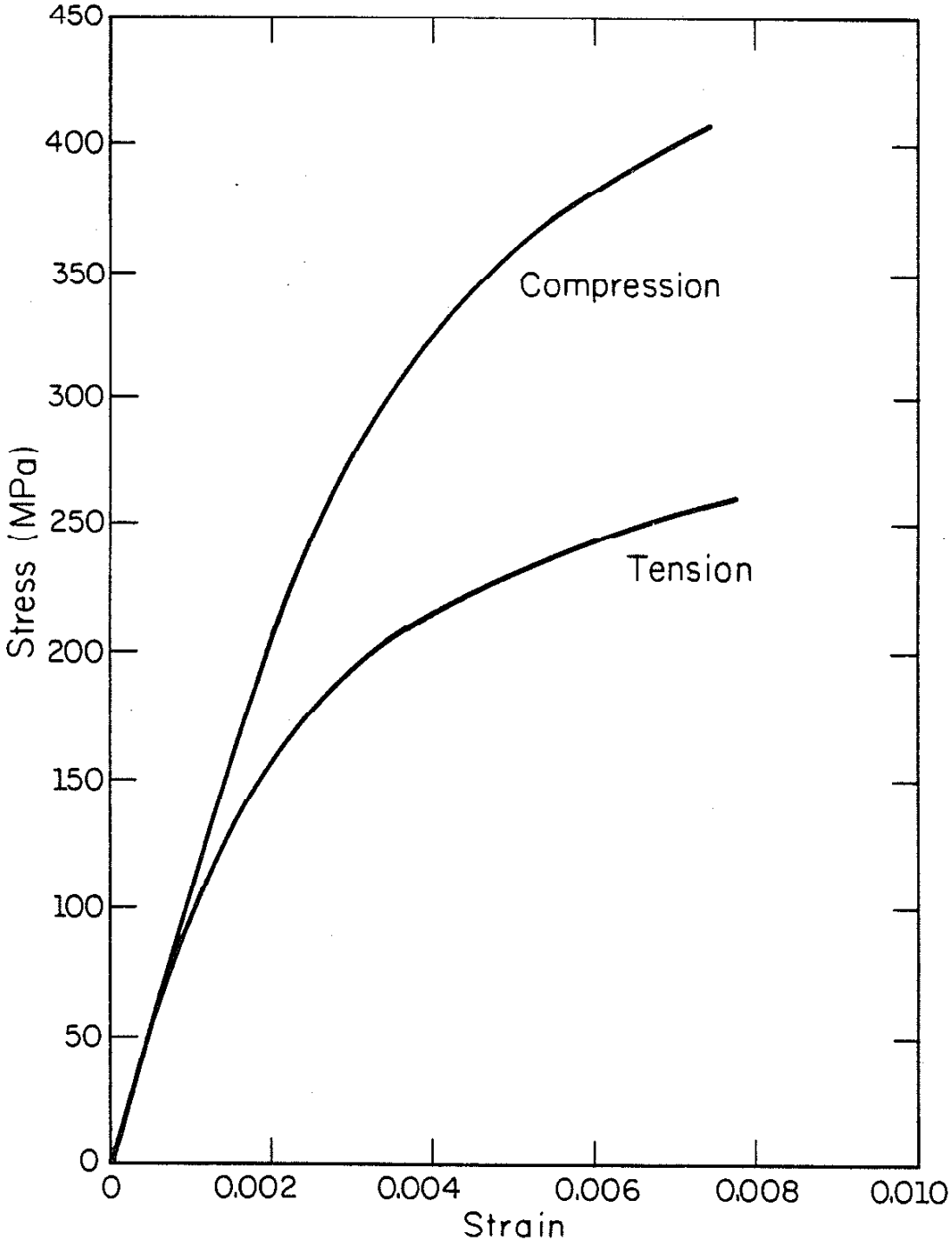

Figure 11 Typical Monotonic Stress-Strain Response

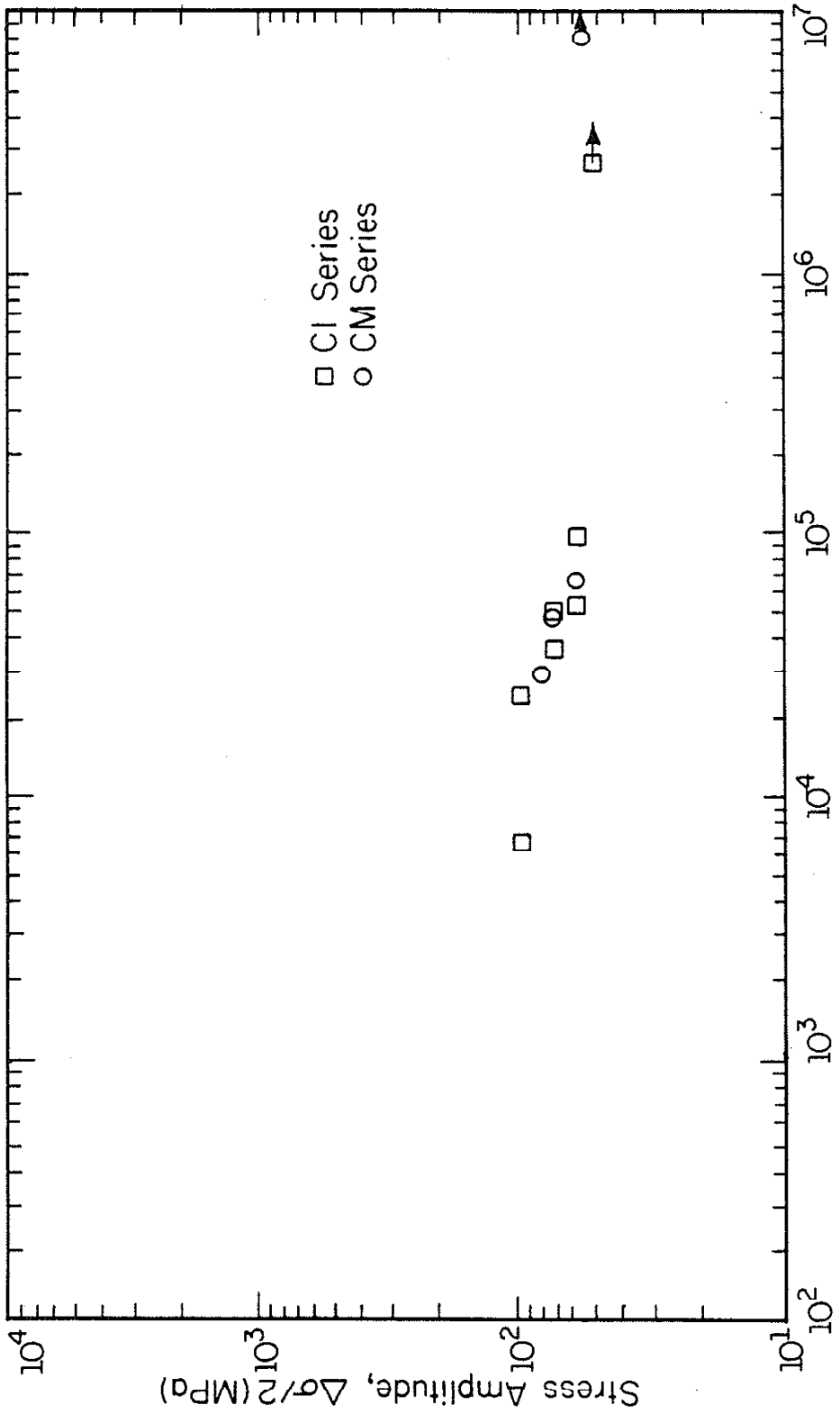

Figure 12 Stress-Life Axial Fatigue Data

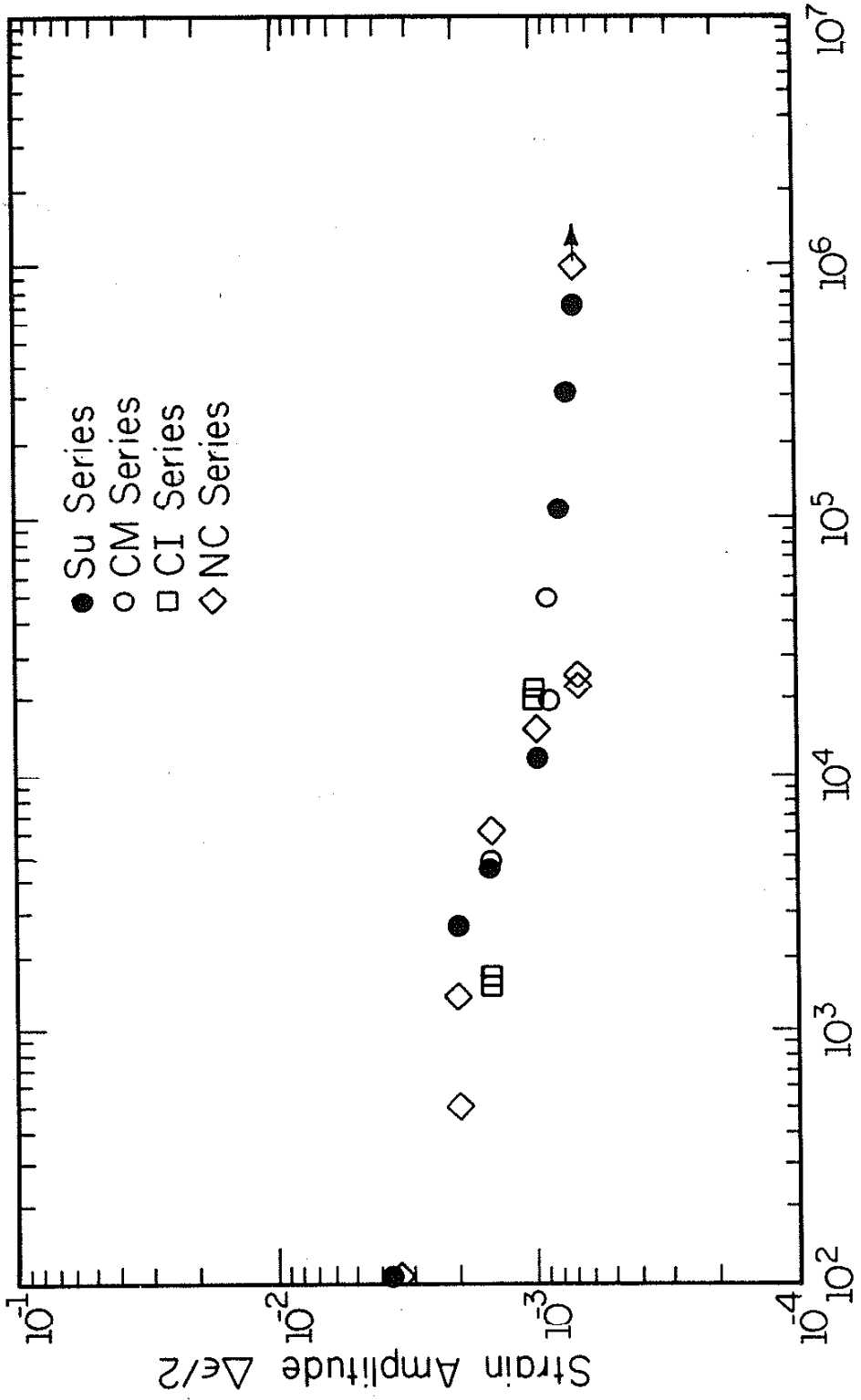

Figure 13 Strain-Life Axial Fatigue Data

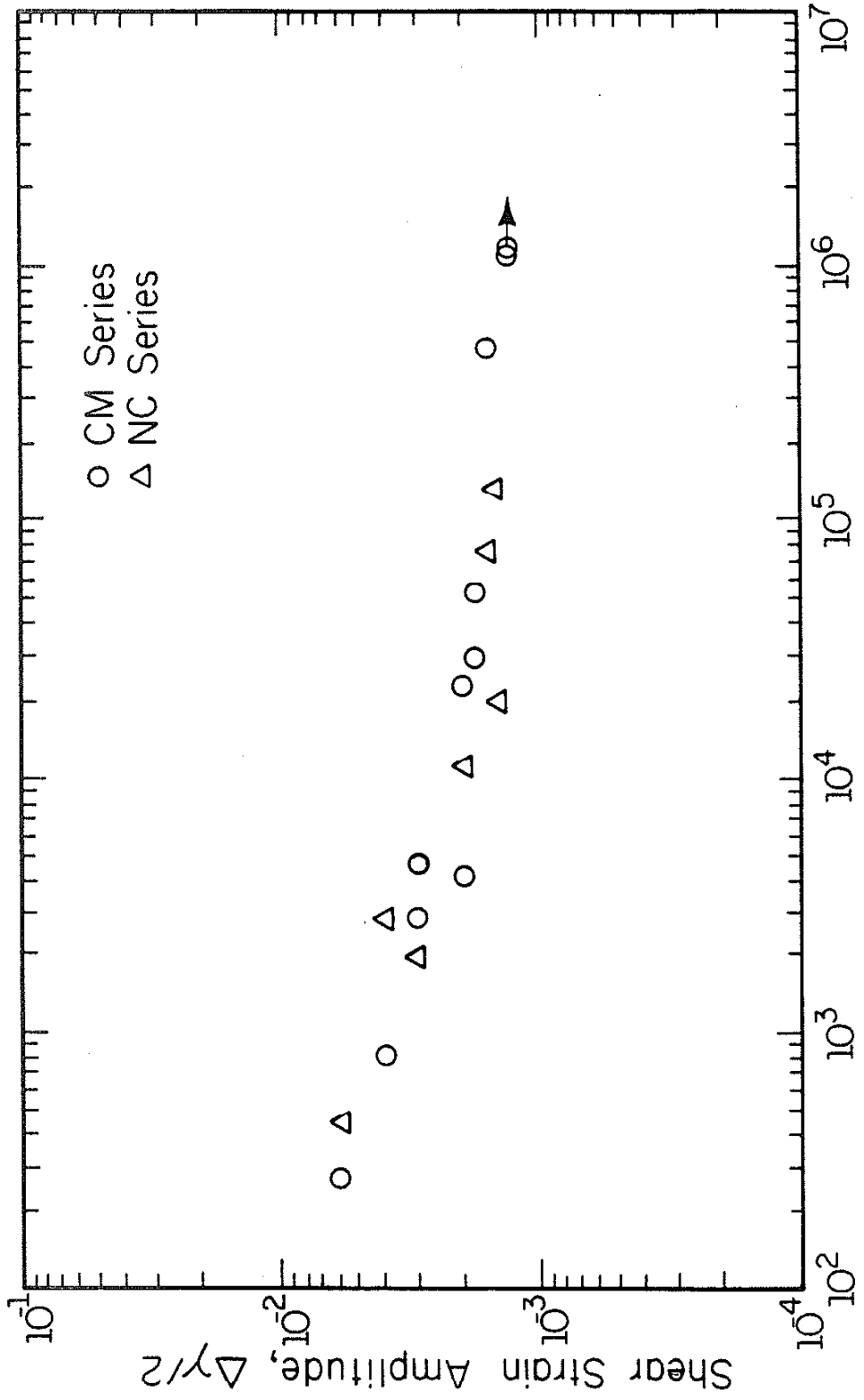

Figure 14 Strain-Life Torsional Fatigue Data

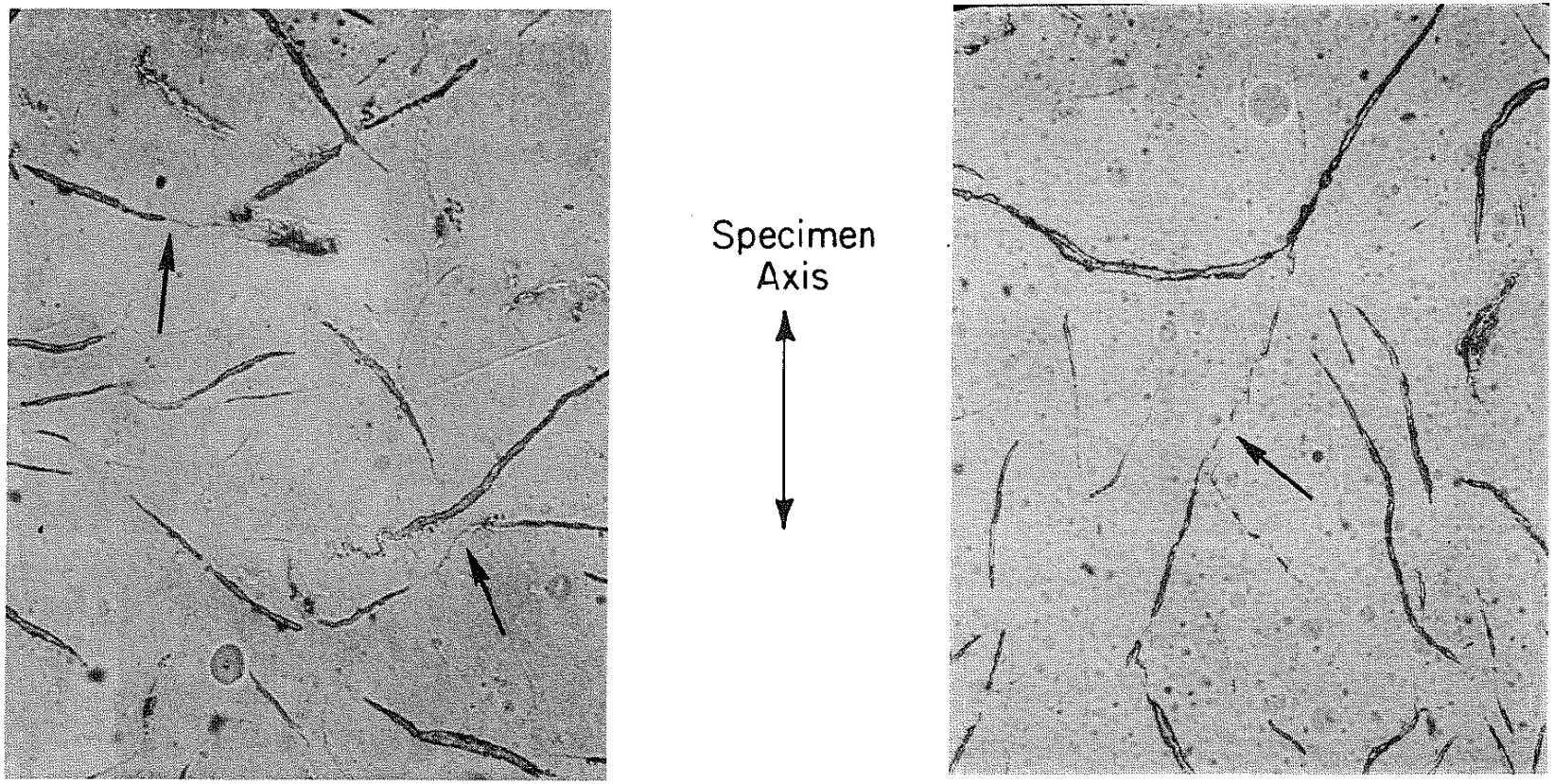

Axial (CM20)

Torsion (CM13)

Figure 15 Crack Initiation from Graphite Flakes

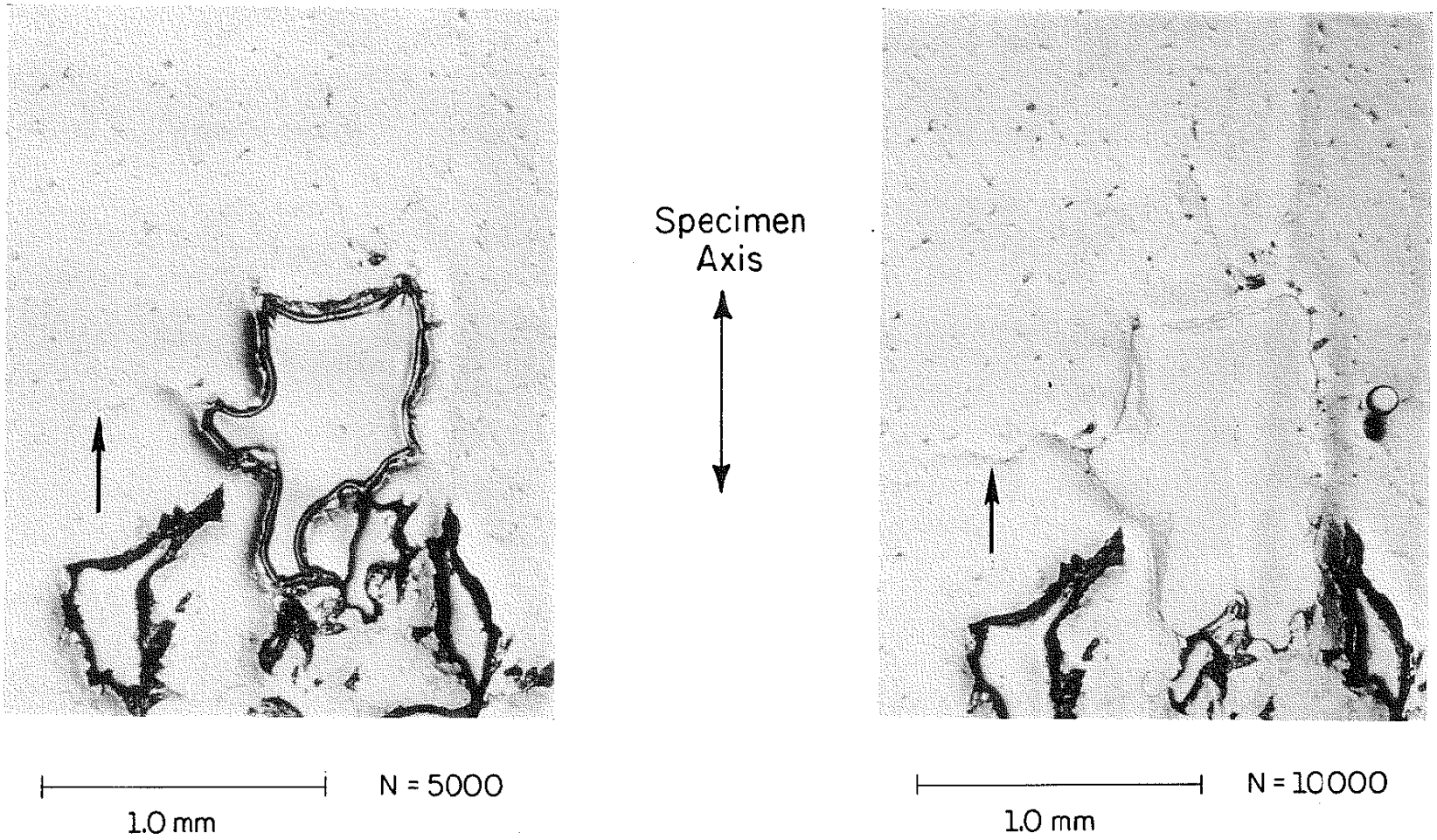

Axial-CM17 $\Delta\epsilon/2 = 0.0009$ $R_\epsilon = -1$ $N_f = 19870$

Figure 16A Crack Initiation and Growth from Defect-Axial Test

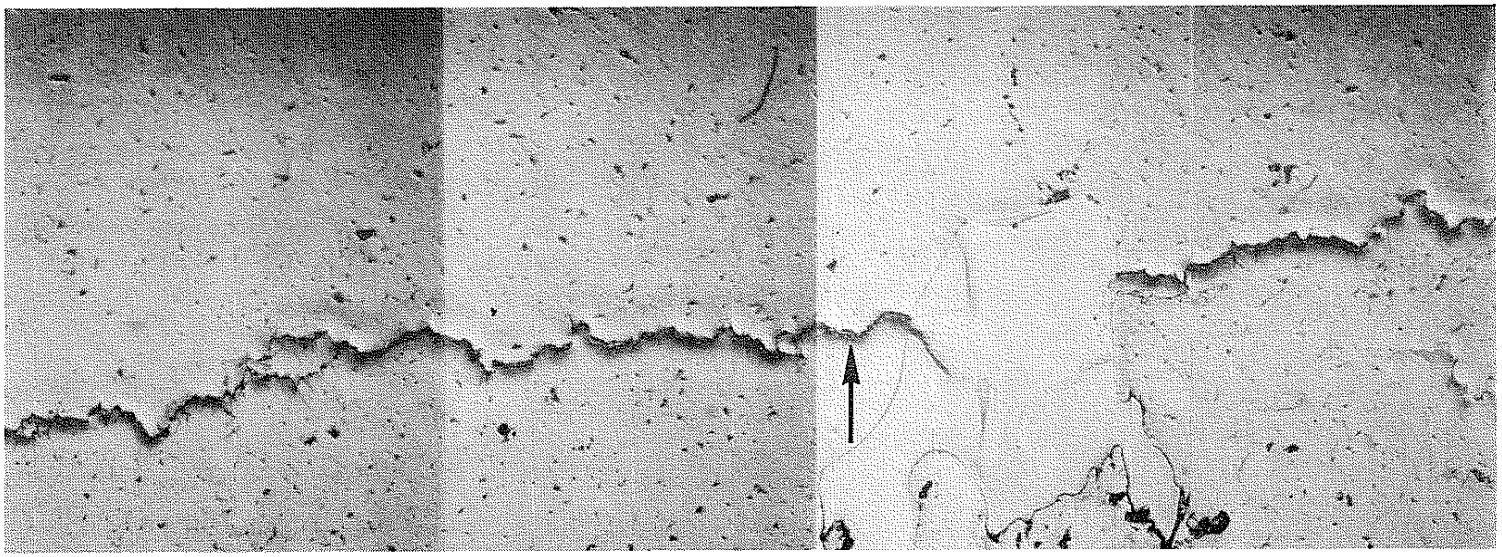

Figure 16B Crack Initiation and Growth from Defect-Axial Test

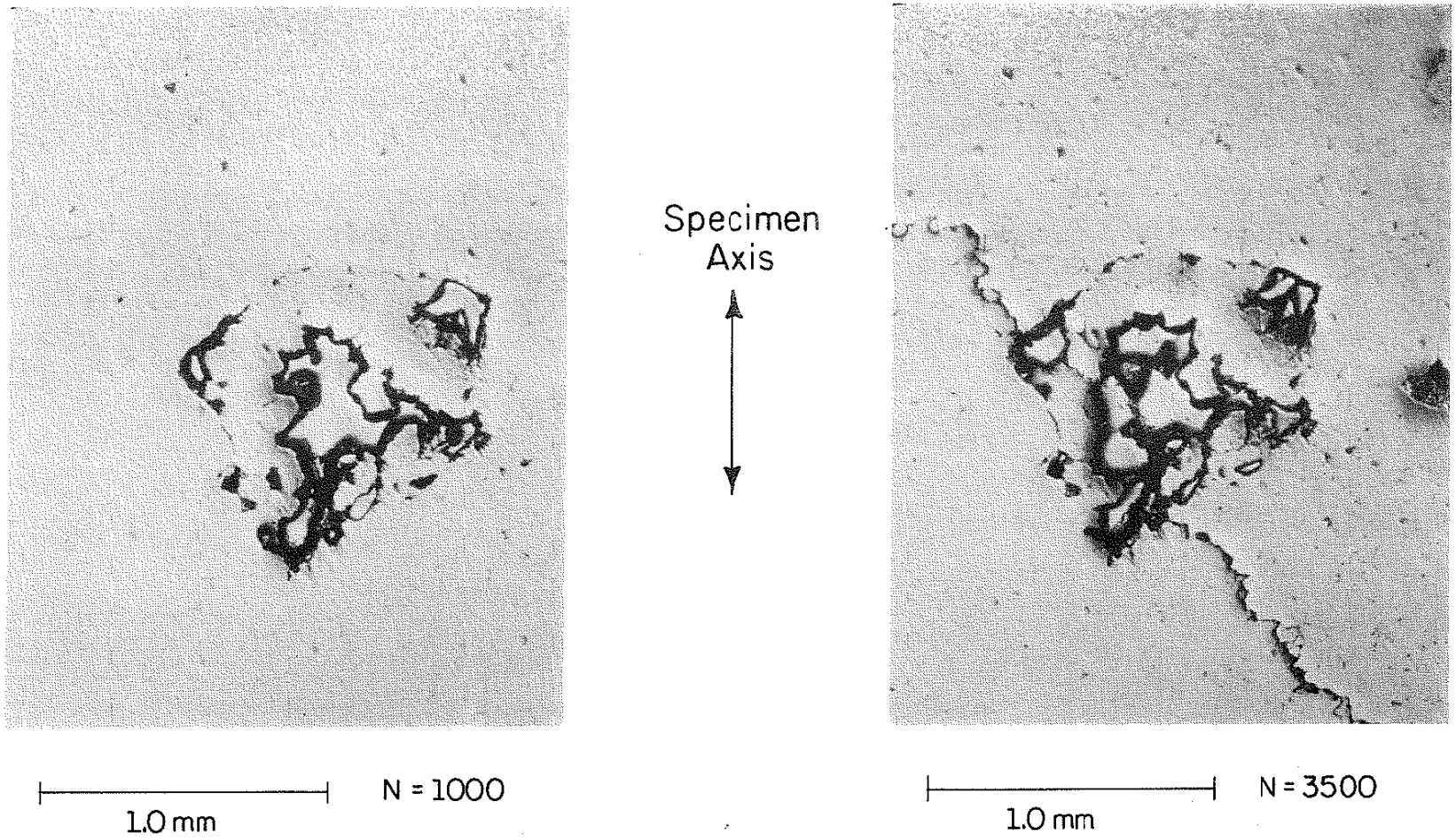

Torsion - CM06 $\Delta\gamma/2 = 0.002$ $R_\gamma = -1$ $N_f = 4020$

Figure 17A Crack Initiation and Growth from Defect-Torsion Test

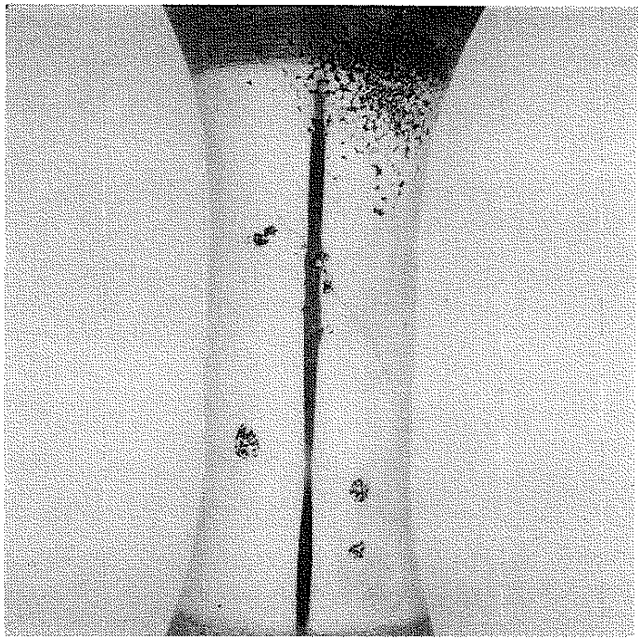

25 mm

Torsion - CM06

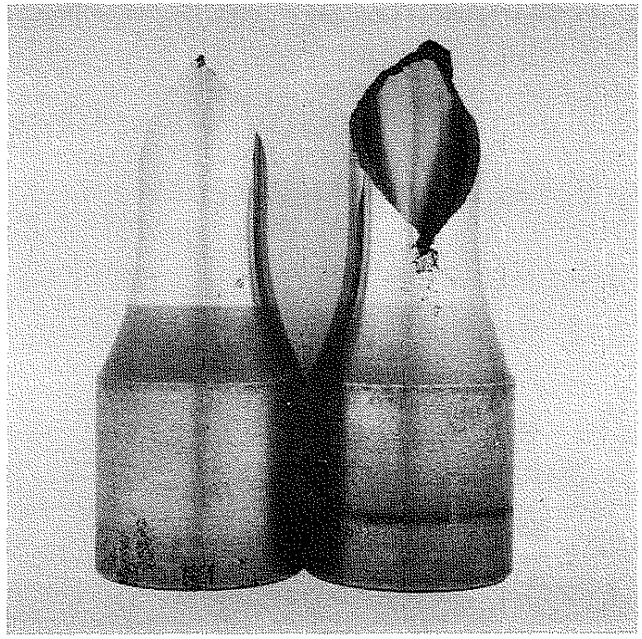

25mm

Torsion - NC08

Figure 17B Crack Initiation and Growth from Defect-Torsion Test

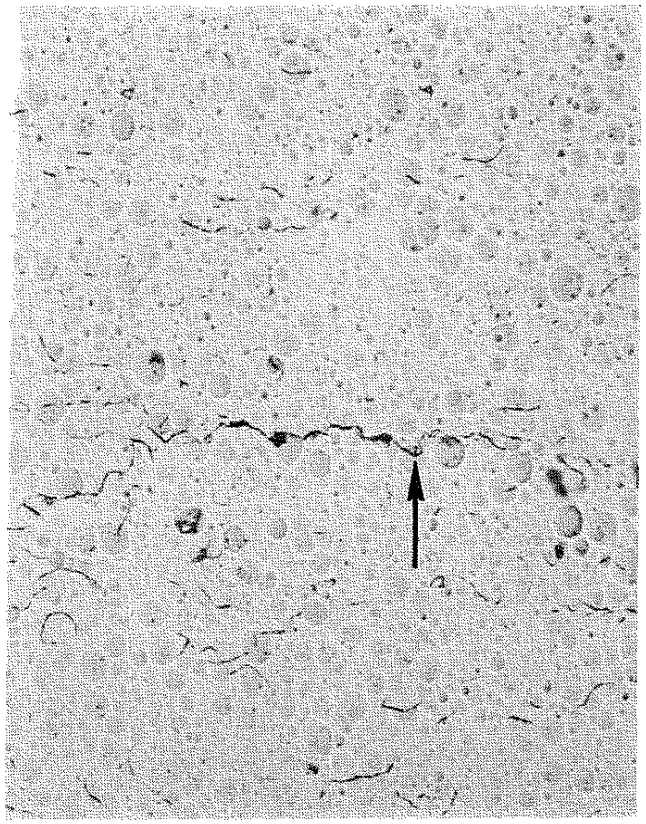

0.2 mm

N = 850

Specimen Axis

Axial - NC18 $\Delta\epsilon/2 = 0.002$ $R_\epsilon = -1$ $N_f = 1340$

Figure 18A Crack Growth for Axial Test - NC18

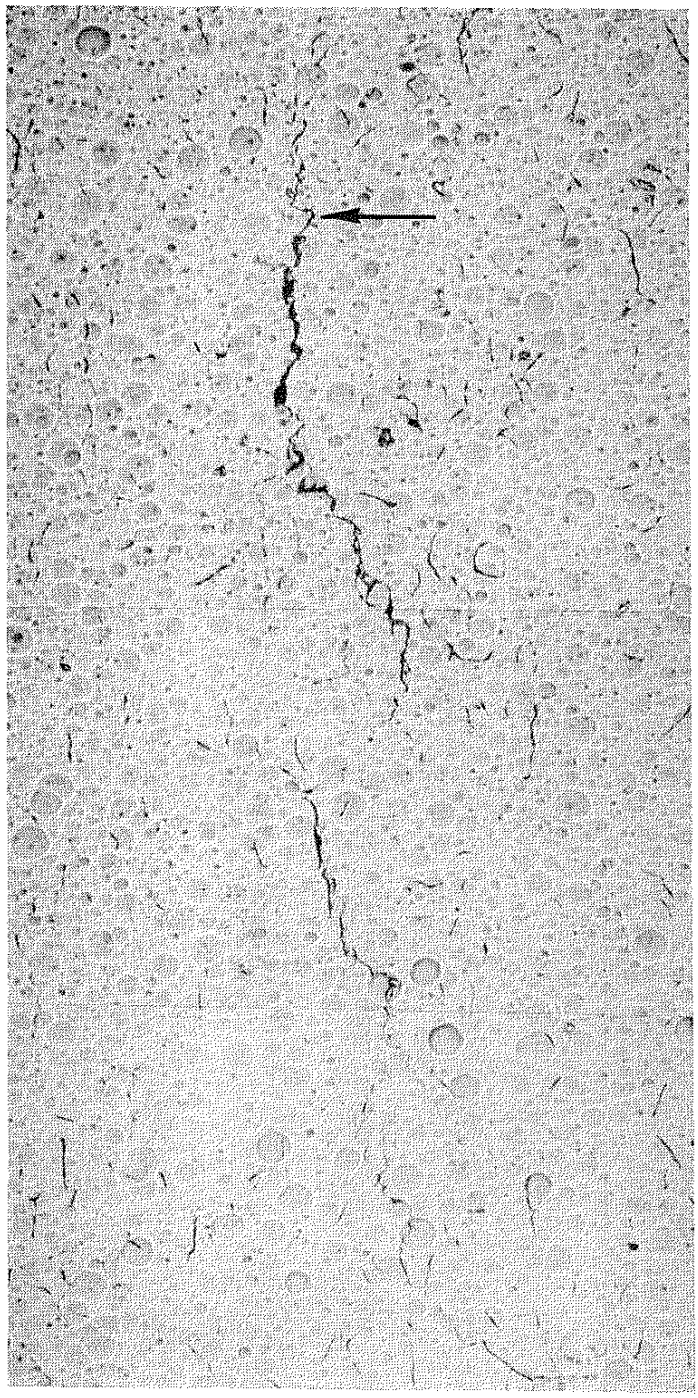

Axial-NC18 $\Delta\epsilon/2 = 0.002$ $R_\epsilon = -1$ $N_f = 1340$

N=1000

0.2 mm

Specimen Axis

Figure 18B Crack Growth for Axial Test - NC18

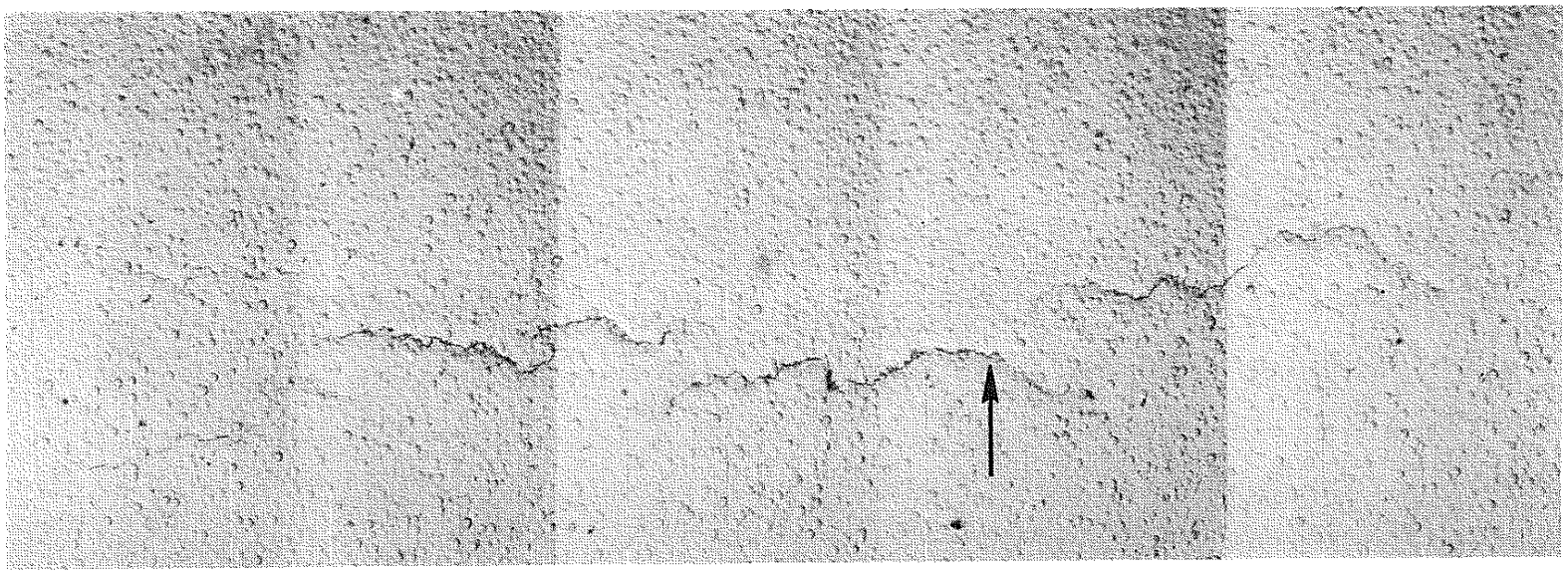

1.0 mm

N=1250

Specimen Axis

Axial-NC18 $\Delta\epsilon/2=0.002$ $R_\epsilon=-1$ $N_f=1340$

Figure 18C Crack Growth for Axial Test - NC18

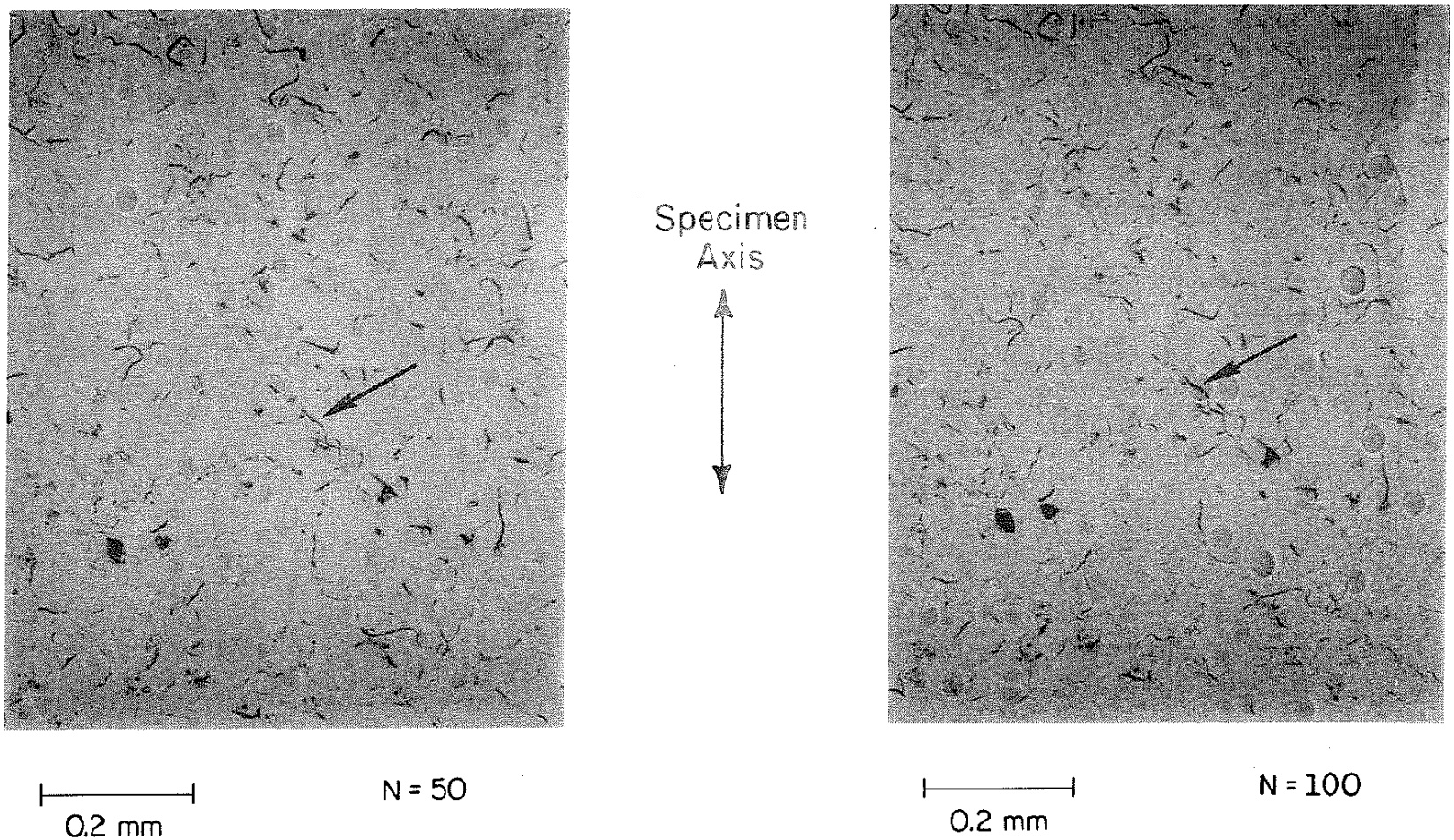

Torsion - NC01 $\Delta\gamma/2 = 0.006$ $R_\gamma = -1$ N = 444

Figure 19A Crack Growth for Torsion Test - NC01

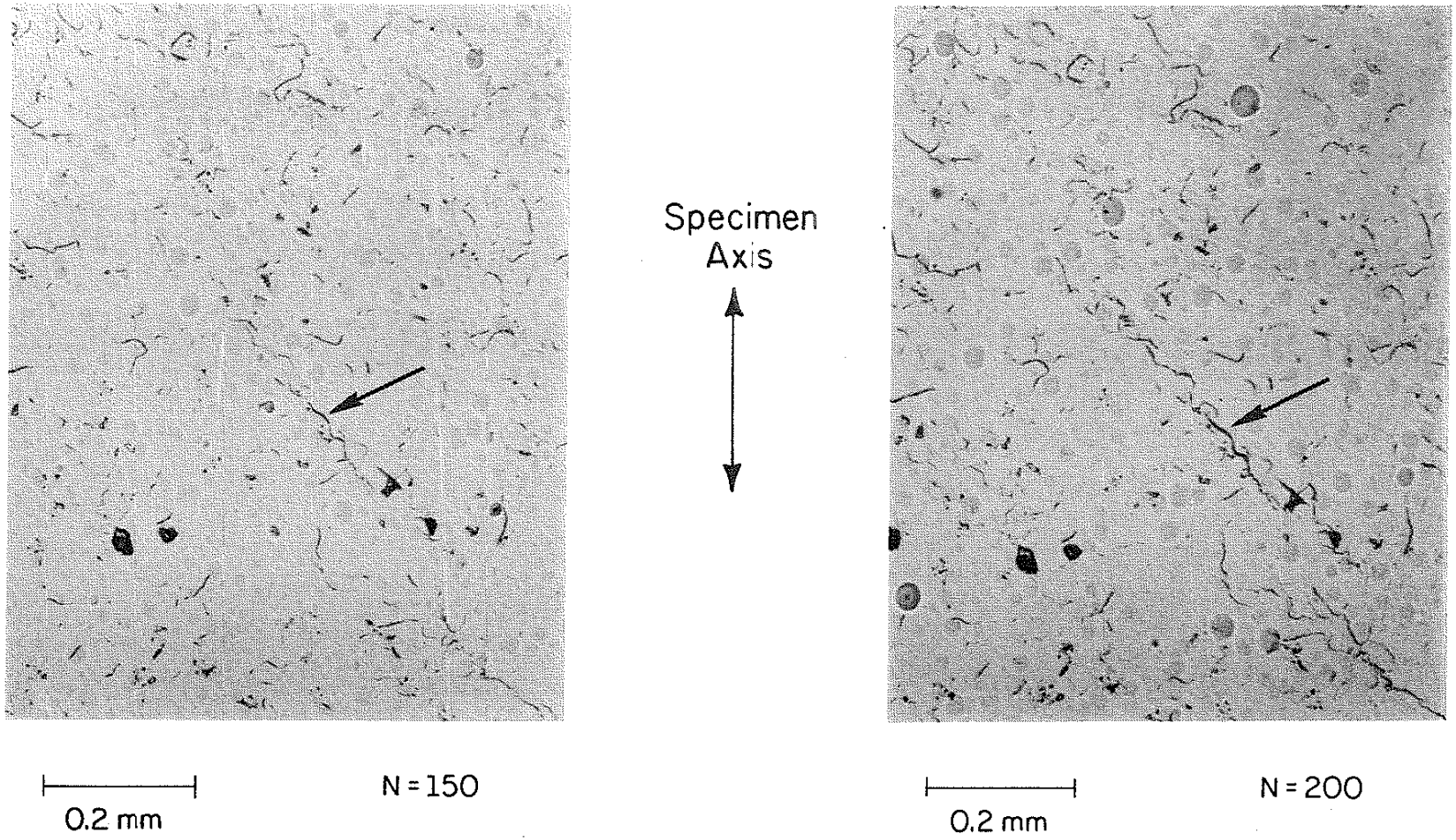

Torsion-NC01 $\Delta\gamma/2 = 0.006$ $R_\gamma = -1$ $N_f = 444$

Figure 19B Crack Growth for Torsion Test - NC01

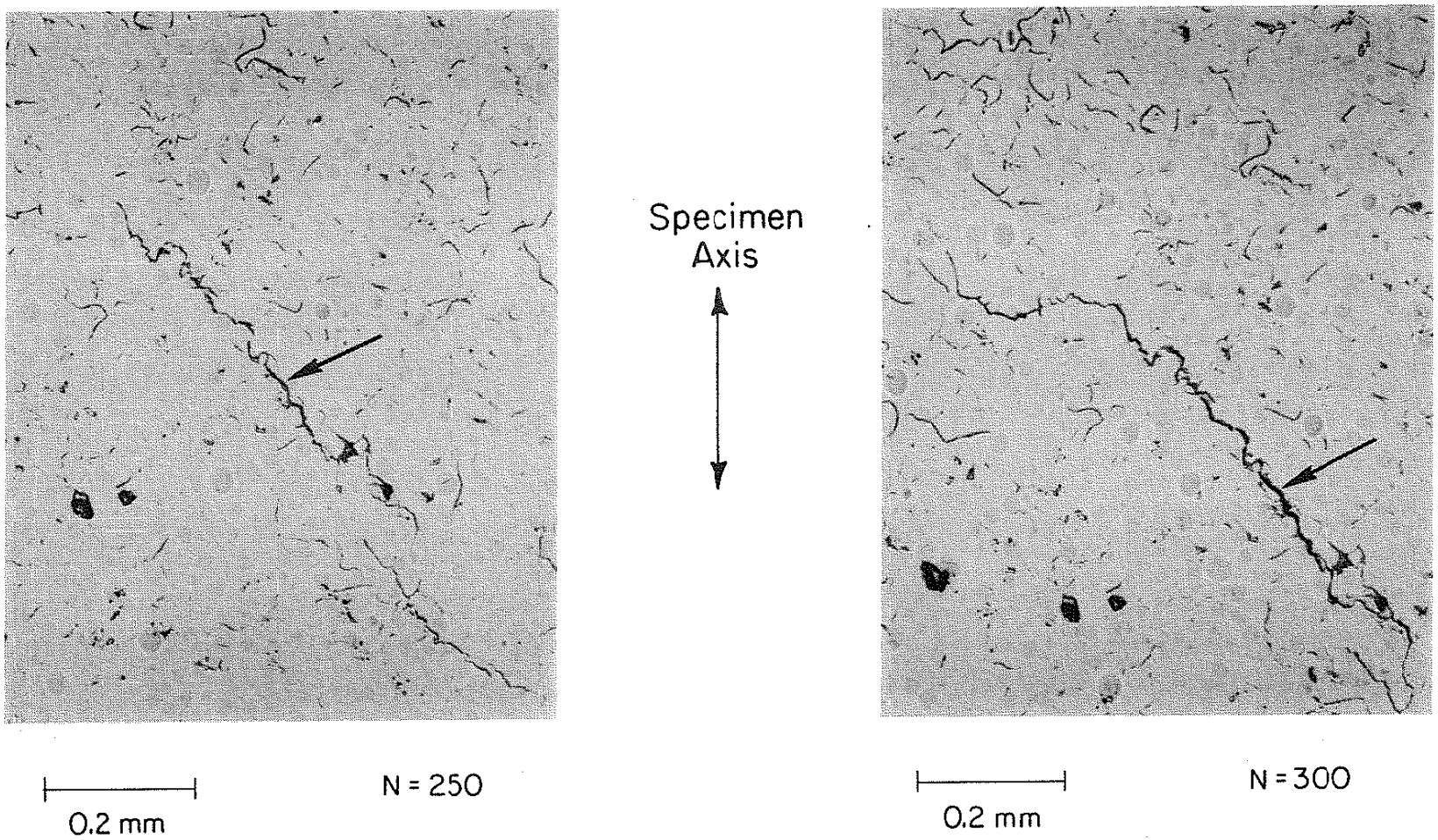

Torsion - NC01 $\Delta\gamma/2 = 0.006$ $R_\gamma = -1$ $N_f = 444$

Figure 19C Crack Growth for Torsion Test - NC01

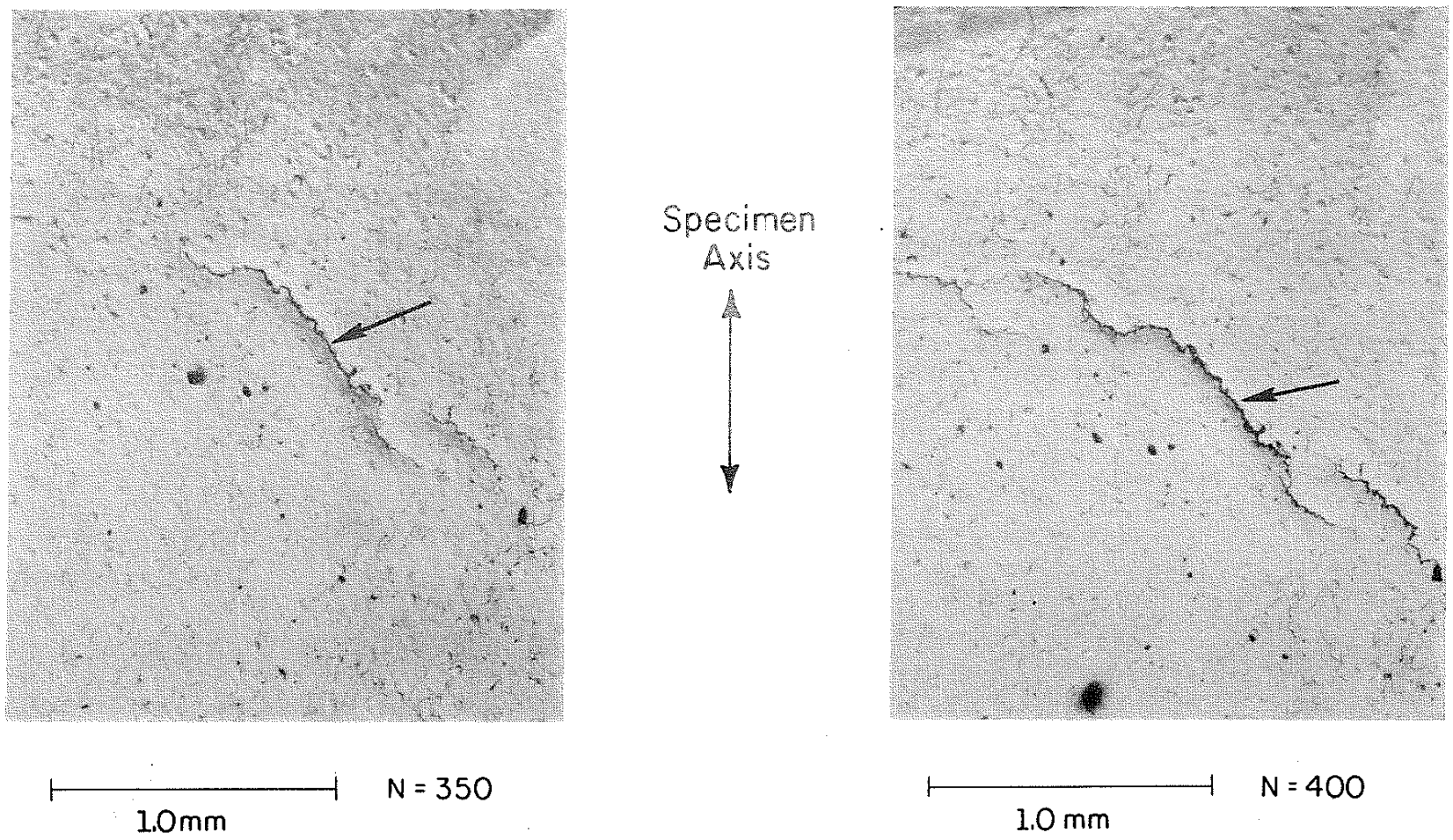

Torsion - NC01 $\Delta\gamma/2 = 0.006$ $R_\gamma = -1$ $N_f = 444$

Figure 19D Crack Growth for Torsion Test - NC01

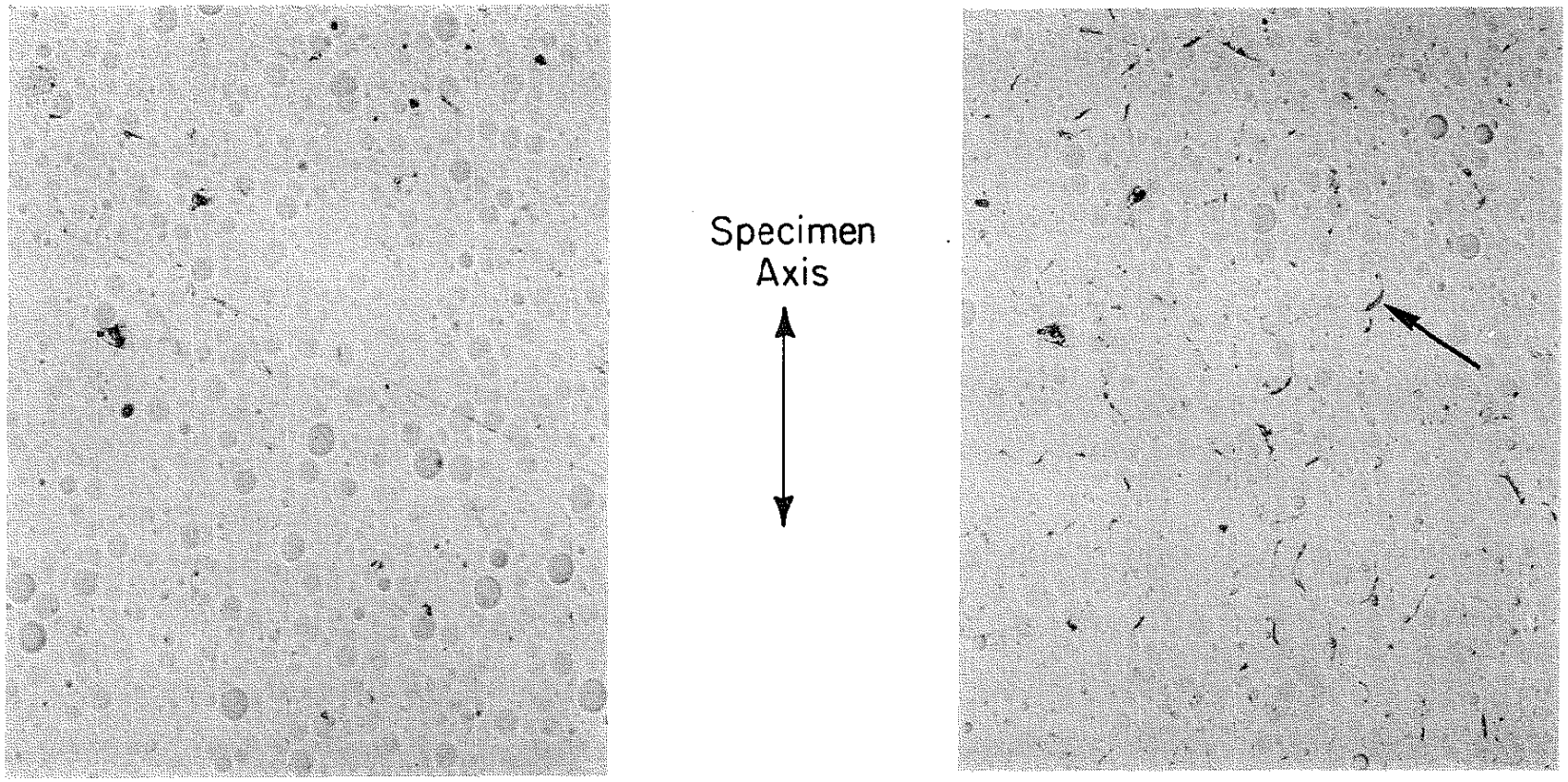

Torsion - NC06 $\Delta\gamma/2 = 0.002$ $R_\gamma = -1$ $N_f = 11000$

Figure 20A Crack Growth for Torsion Test - NC06

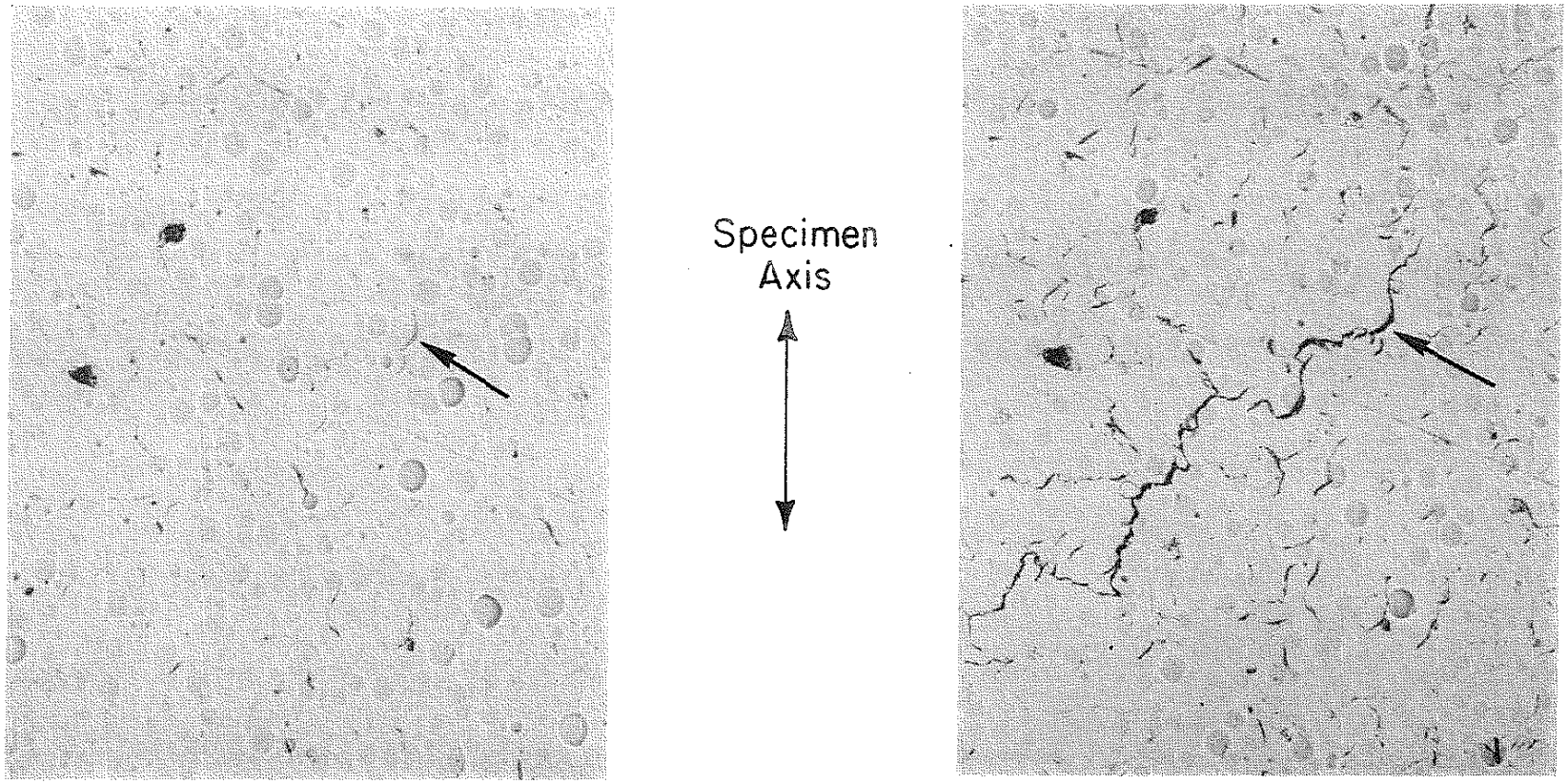

Torsion - NC06 $\Delta\gamma/2 = 0.002$ $R_\gamma = -1$ $N_f = 11000$

Figure 20B Crack Growth for Torsion Test - NC06

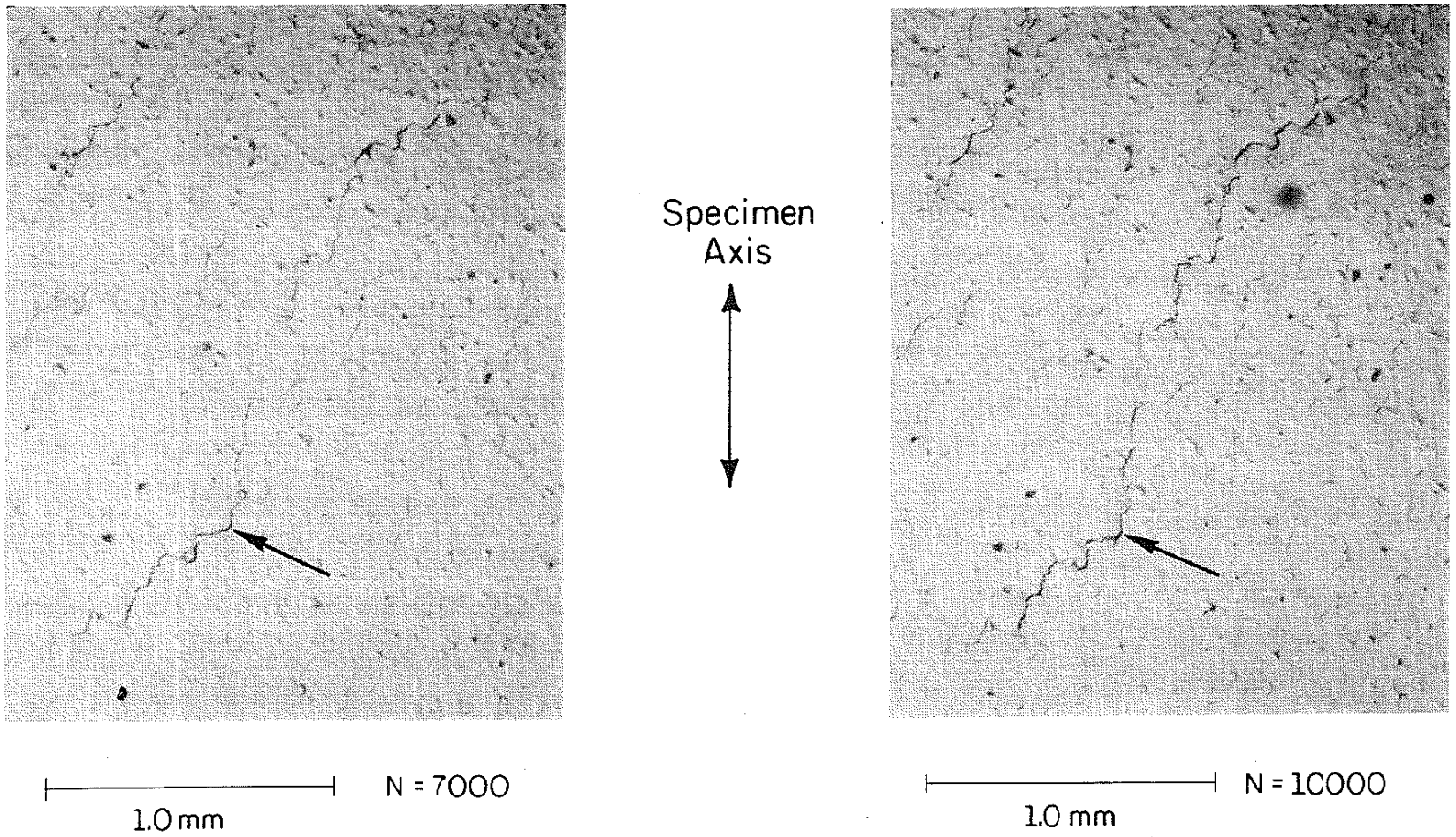

Torsion - NC06 $\Delta\gamma/2 = 0.002$ $R_\gamma = -1$ $N_f = 11000$

Figure 20C Crack Growth for Torsion Test - NC06

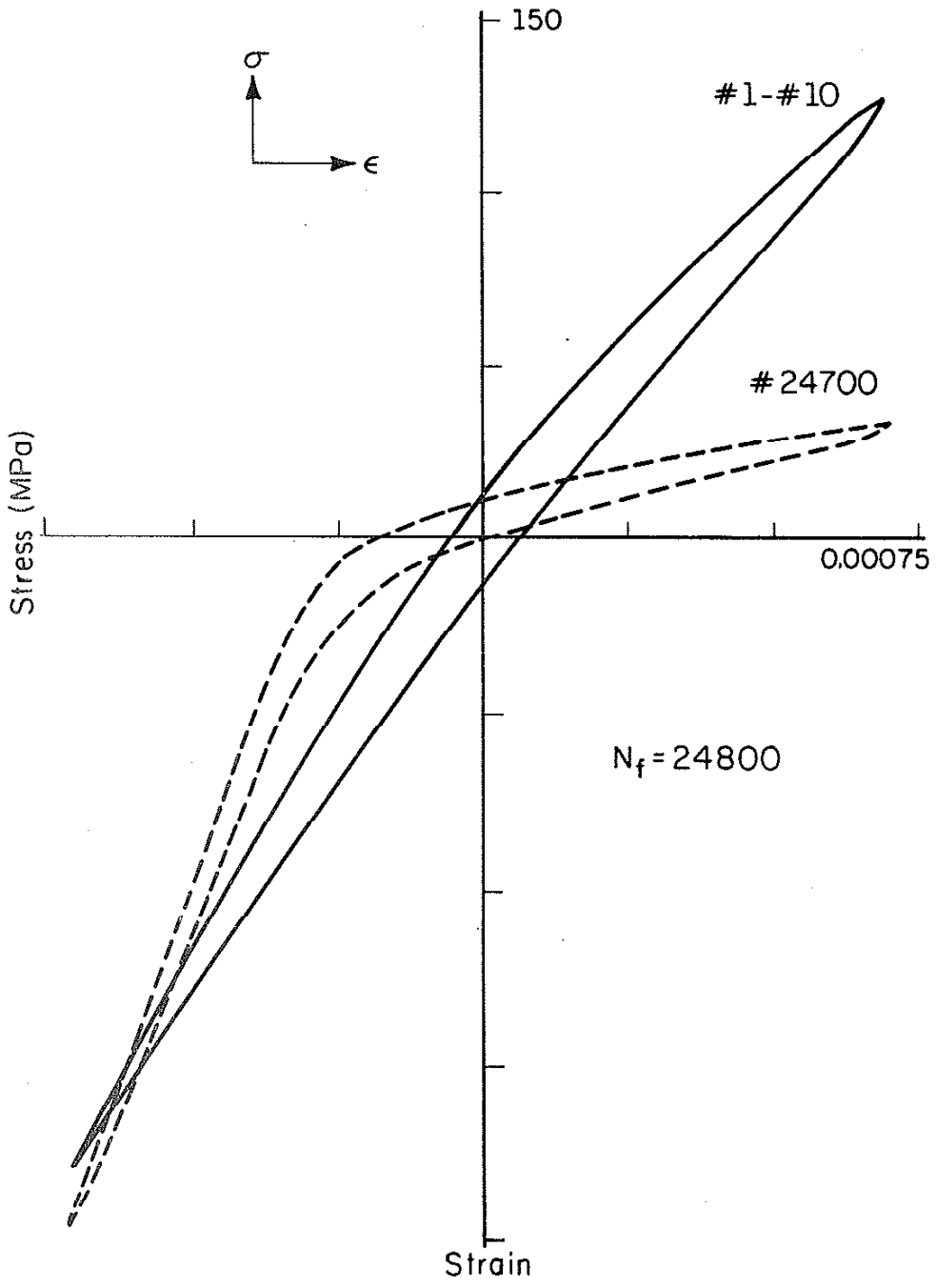

Figure 21 Hysteresis Response-Axial Test; $\Delta\varepsilon/2 = 0.0007$

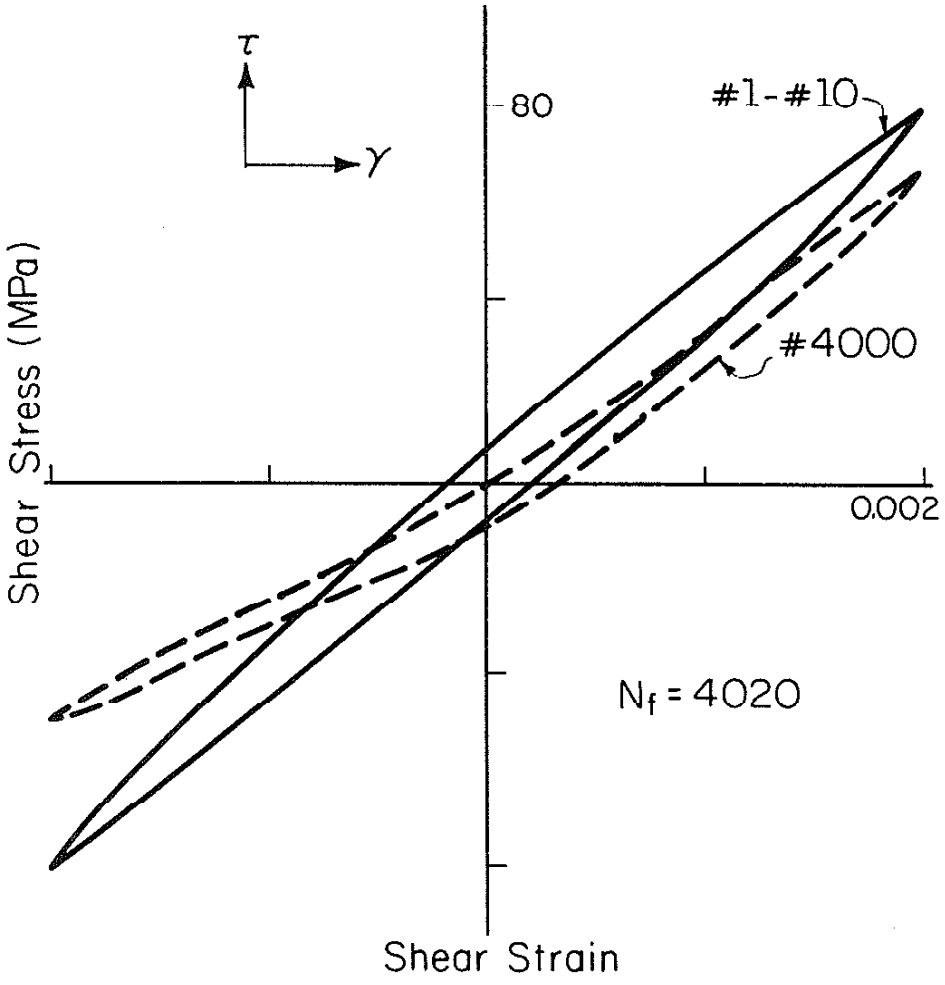

Figure 22 Hysteresis Response-Torsion Test; $\Delta\gamma/2 = 0.002$

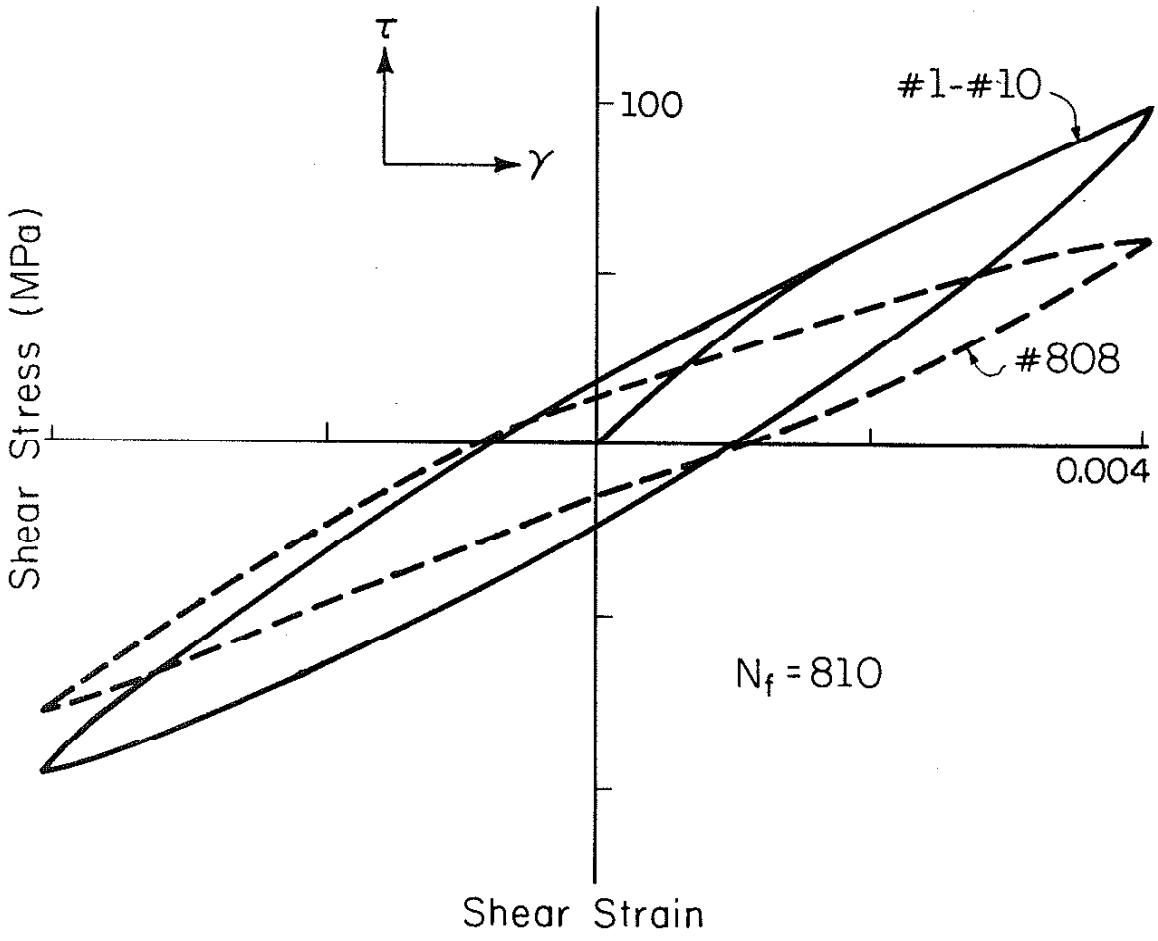

Figure 23 Hysteresis Response-Torsion Test; $\Delta\gamma/2 = 0.004$

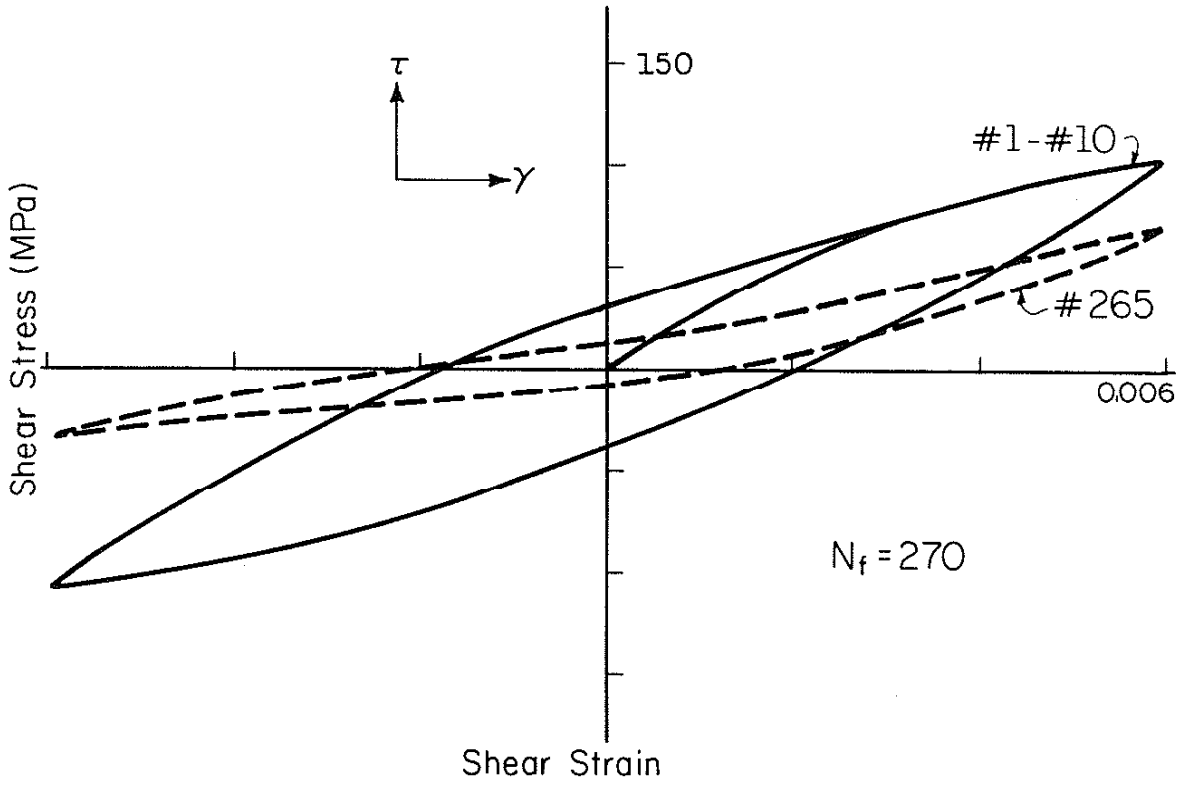

Figure 24 Hysteresis Response-Torsion Test; $\Delta\gamma/2 = 0.006$

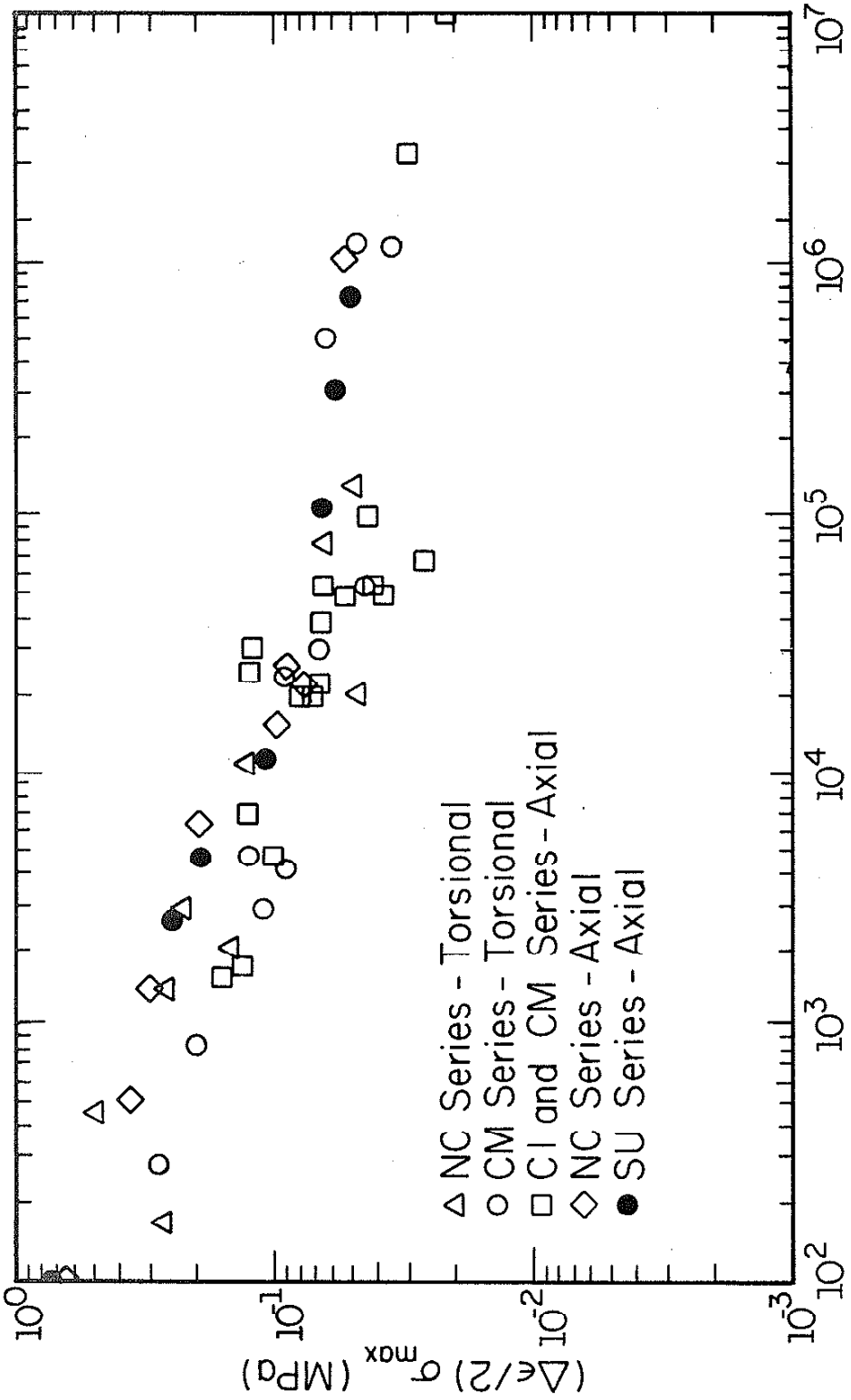

Figure 25 SWT Presentation of Fatigue Test Results

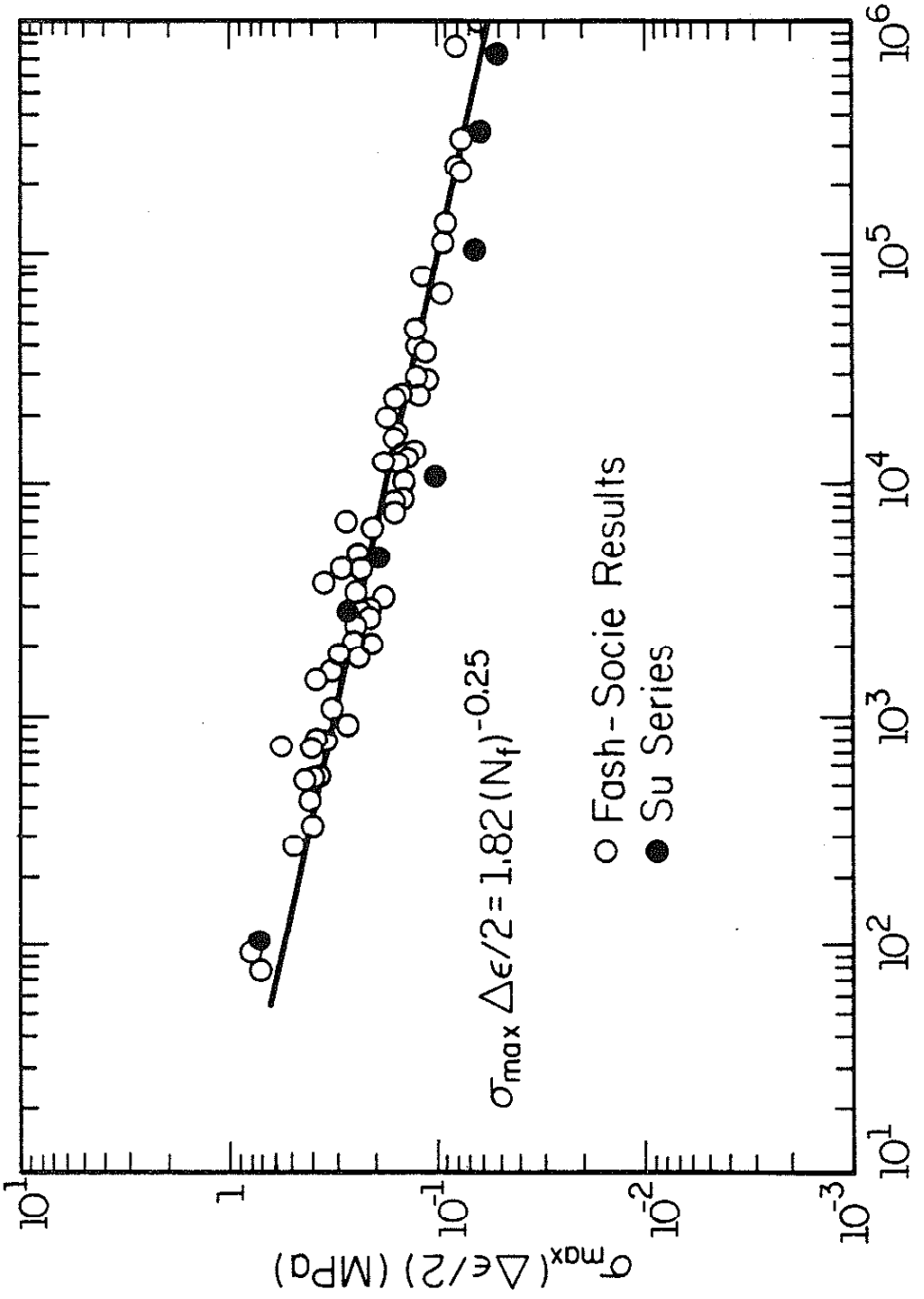

Figure 26 SWT Presentation of Fash-Socie Results

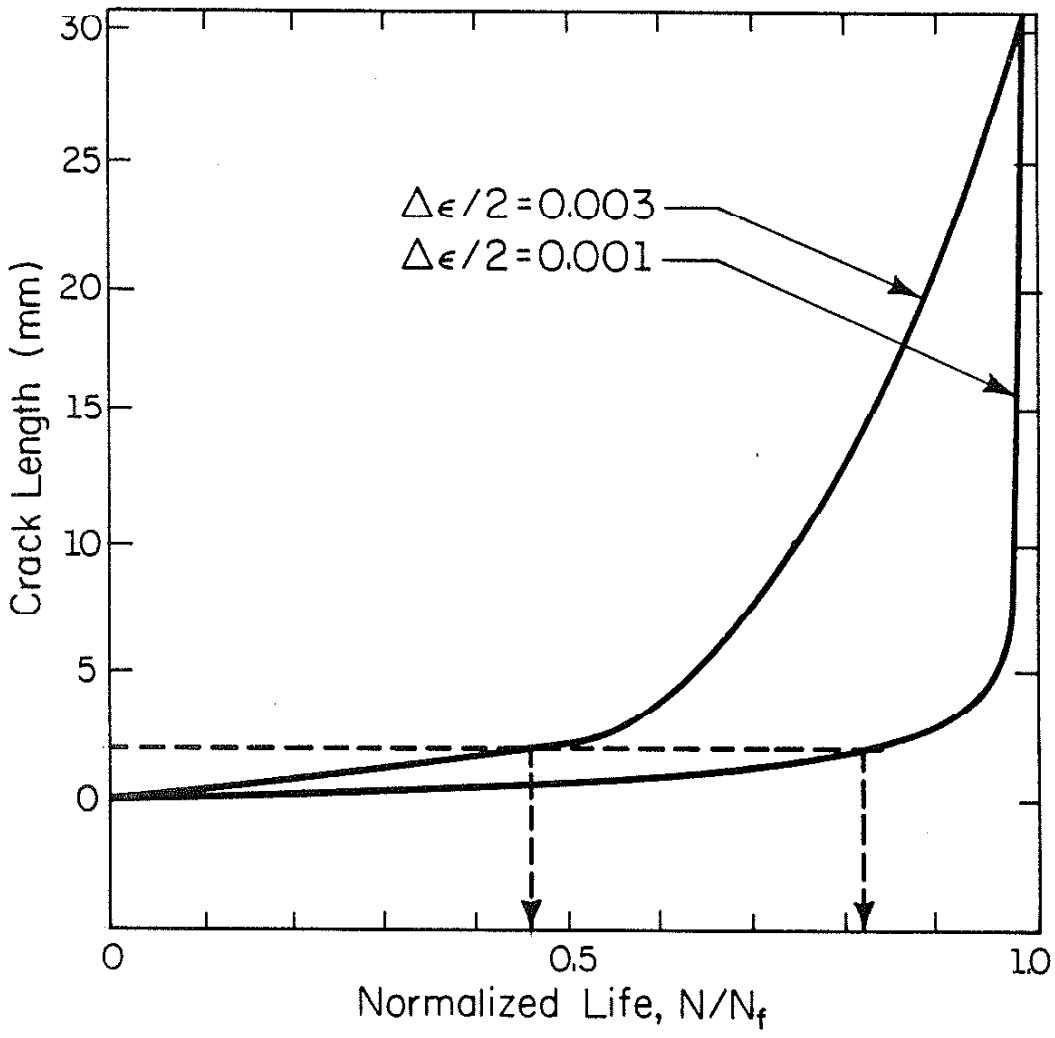

Figure 27 Damage Plot: Crack Length versus Normalized Life

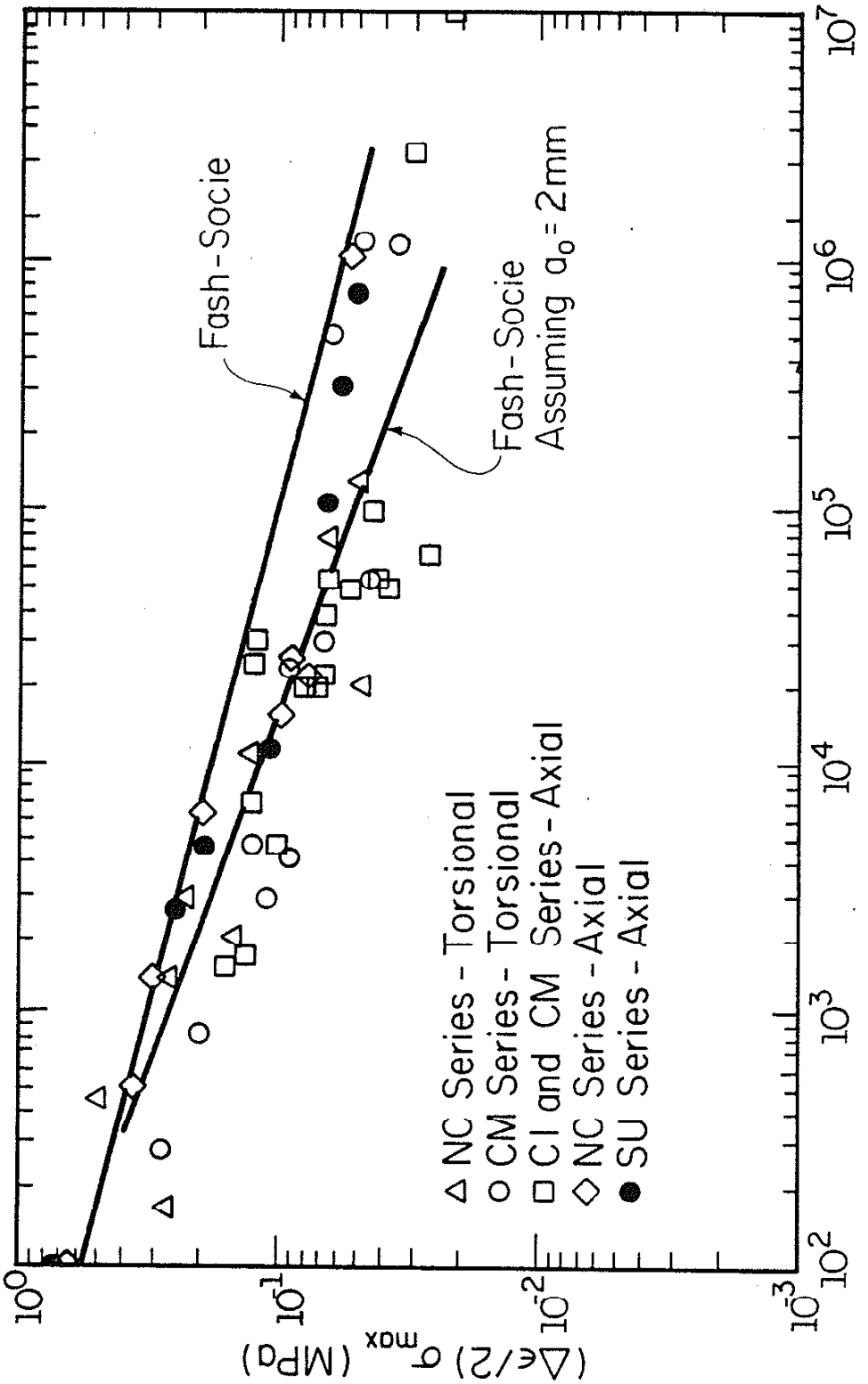

Figure 28 SWT Presentation with 2 mm Defect Line

REFERENCES

1. Thum, A., and Ude, H., "Die Elastizitat und die Schwingungsfestigkeit des Gusseisens," Die Giesserei, Vol. 16, 1929, pp. 547-556.

2. Coffin, L. F., Jr., "The Flow and Fracture of a Brittle Material," Journal of Applied Mechanics, American Society of Mechanical Engineers, Vol. 17, No. 3, September 1950, p. 74.

3. Clough, W. R., and Shank, M. E., "The Deformation and Rupture of Gray Cast Iron," Transactions of the American Society for Metals, Vol. 49, 1957, pp. 241-262.

4. Gilbert, G. N. J., "The Components of Strain Due to Deformation of the Matrix and Due to Volume Changes in a Flake Graphite Cast Iron Under Uniaxial Stress," Journal of the British Cast Iron Research Association, Vol. 11, 1963, pp. 512-524.

5. Gilbert, G. N. J., "Variations of the Microstructure of a Flake Graphite Cast Iron after Stressing in Tension and Compression," Journal of the British Cast Iron Research Association, Vol. 12, 1964, pp. 31-47.

6. Gilbert, G. N. J., "Factors Relating to the Stress-Strain Properties of Cast Iron," Journal of the British Cast Iron Research Association, Vol. 6, 1957, pp. 546-588.

7. Ikawa, K., and Ohira, G., "Fatigue Properties of Cast Iron in Relation to Graphite Structure," American Foundry Society, Cast Metals Research Journal, Vol. 3, No. 1, 1967, pp. 11-21.

8. Mitchell, M. R., "Effects of Graphite Morphology, Matrix Hardness, and Structure on the Fatigue Resistance of Gray Cast Iron," Society of Automotive Engineers, Inc., Report No. 750198, 1975, 13 pp.

9. Fash, J. W., "Fatigue Crack Initiation and Growth in Gray Cast Iron," Fracture Control Program, Report No. 35, College of Engineering, University of Illinois at Urbana-Champaign, October 1980.

10. Furman, P. J., "Fatigue Behavior of Gray Cast Iron Under Axial and Bending Loads," Materials Engineering-Mechanical Behavior, Report No. 119, College of Engineering, University of Illinois at Urbana-Champaign, May 1985.

11. Forsyth, P. J. E., "A Two-Stage Process of Fatigue Crack Growth," Proceedings, Crack Propagation Symp., Cranfield, 1961, pp. 76-94.

12. Smith, K. N., Watson, P., and Topper, T. H., "A Stress-Strain Function for the Fatigue of Metals," Journal of Materials, Vol. 5, No. 4, December 1970, pp. 767-778.

13. Fash, J. W., and Socie, D. F., "Fatigue Behavior and Mean Effects in Gray Cast Iron," International Journal of Fatigue, Vol. 4, No. 3, 1982, pp. 137-142.

14. Draffin, J. O., and Collins, W. L., "Effect of Size and Type of Specimen on the Torsional Properties of Cast Iron," Proceedings, American Society for Testing and Materials, Vol. 38, Part II, 1938, pp. 235-248.

15. Draffin, J. O., Collins, W. L., and Casberg, C. H., "Mechanical Properties of Gray Cast Iron in Torsion," Proceedings, American Society for Testing and Materials, Vol. 40, 1940, pp. 840-848.

16. Grassi, R. C., and Cornet, I., "Fracture of Gray-Cast-Iron Tubes Under Biaxial Stresses," Journal of Applied Mechanics, American Society for Mechanical Engineers, Vol. 71, 1949, pp. 178-182.

17. Sylvia, J. G., Cast Metals Technology, Addison-Wesley Publishing Company, Inc., 1972, pp. 46-49.

18. Walton, C. F., ed., Gray and Ductile Iron Castings Handbook, The Gray and Ductile Iron Founders' Society, Inc., 1971, pp. 14-15.

19. "Standard Method for Evaluating the Microstructure of Graphite in Iron Castings, A247," 1985 Annual Book of ASTM Standards, Section 1, Vol. 1.02, Ferrous Castings, American Society for Testing and Materials, 1985, pp. 141-143.

20. Waill, L. E., "Crack Observations in Biaxial Fatigue," Design and Materials Division, Report No. 108, Department of Mechanical and Industrial Engineering, University of Illinois at Urbana-Champaign, March 1983.

21. Downing, S. D., "Modeling Cyclic Deformation and Fatigue Behavior of Cast Iron Under Uniaxial Loading," Materials Engineering-Mechanical Behavior, Report No. 101, College of Engineering, University of Illinois at Urbana-Champaign, January 1984.

22. Lemaitre, J., and Plumtree, A., "Application of Damage Concepts to Predict Creep-Fatigue Failures," Journal of Engineering Materials and Technology, American Society of Mechanical Engineers, Vol. 101, July 1979, pp. 284-292.

23. Socie, D. F., Fash, J. W., and Leckie, F. A., "A Continuum Damage Model for Fatigue Analysis of Cast Iron," Proceedings, ASME International Conference on Advances in Life Prediction Methods, D. A. Woodford and J. R. Whitehead, eds., The American Society of Mechanical Engineers, Albany, New York, 1983, pp. 59-64.